EXPLORING THE THERAPEUTIC POTENTIAL OF UROLITHIN A FOR HEALTHY AGEING: IN SILICO STUDY

Caroline Alphonce Massanga

A Dissertation Submitted in Partial Fulfilment of the Requirements for the Degree of Master of Science in Human Nutrition and Dietetics of the Nelson Mandela African Institution of Science and Technology

Arusha, Tanzania

August, 2025

ABSTRACT

Urolithin A, an active precursor derived from the metabolism of ellagitannins in rats and humans, is known for its potential health benefits, including stimulating mitophagy and promoting musculoskeletal function. While experimental studies have demonstrated Urolithin A's potential to enhance cellular health, the detailed molecular interactions through which Urolithin A exerts its effects are not fully elucidated. Hence, this study investigated the anti-inflammatory, anti-oxidation and neuro-protective abilities of Urolithin A in selected targets using molecular docking and molecular dynamics simulation methods. Molecular docking studies revealed the strong affinity for receptors involved in inflammation activities, including human p38 MAP kinase (4DLI) with ¯10.1 kcal/mol interacting with SER^{252}, LYS^{249} and ASP^{294} residues. The binding energy in the 5KIR target was ¯8.6 kcal/mol, interacting with GLN^{203} through hydrogen bond, and lastly, 1A9U with an affinity of ¯6.8 with no hydrogen bond formed with Urolithin A and interacts with van der Waals interactions. In oxidative targets, the influence of Urolithin A was observed in 1OG5 with ¯7.9 kcal/mol interacting with GLN^{185}, PHE^{447}. For the 1M17 target, the binding affinity was ¯7.7 kcal/mol, interacting with THR^{95} residue and 1ZXM target at ¯7.4 kcal/mol, interacting with TYR^{36}, TYR^{216}, and LEU^{234} residues. The neuro-protective ability of Urolithin A was observed in selected targets for acetyl cholinesterase; the binding energy was ¯9.7 kcal/mol interacting with van der Waals and π der Waals and π interactions; for the 1GQR target, the binding energy was ¯9.9 kcal/mol interacting with van interactions and for β-amylase (1iyt) the binding energy was ¯5.5 forming hydrogen bond with ^{SER8}, GLN^{15} residues. Molecular Dynamics simulations at 100 ns of Urolithin A compared with reference 4DLI. The Urolithin A-4DLI complex exhibited greater stability than the reference receptor, as confirmed by RMSD, RMSF, Radius of Gyration, Hydrogen bond and SASA analyses.

DECLARATION

I, Caroline Alphonce Massanga, declare to the Senate of the Nelson Mandela African Institution of Science and Technology that this dissertation is my original work and has neither been submitted nor is concurrently submitted for degree award in any other institution.

Caroline Alphonce Massanga Date

The above declaration is confirmed by:

Dr. Jofrey Raymond Date

Prof. Musa Chacha Date

Dr. Sr. John Mary Vianney Date

Dr. Lucas Paul Luchemba Date

COPYRIGHT

CERTIFICATION

The undersigned certify that they have read and hereby recommend for examination the dissertation titled, **"*Exploring the Therapeutic Potential of Urolithin A for Healthy Aging: In Silico Study*"**, in Partial Fulfilment of the Requirements for the Award of the Degree of Master's in Life Sciences of the Nelson Mandela African Institution of Science and Technology, Arusha, Tanzania.

Dr. Jofrey Raymond Date

Prof. Musa Chacha Date

Dr. Sr. John Mary Vianney Date

Dr. Lucas Paul Luchemba Date

ACKNOWLEDGMENTS

I am deeply grateful to the Almighty God, whose steadfast presence guided me throughout this significant journey. Despite encountering challenges along the way, I have reached this point through His boundless love, mercy, and grace.

I also wish to extend my deepest gratitude to my supervisors, Dr. Jofrey Raymond, Dr. Sr. John-Mary Vianney, Prof. Musa Chacha, and Dr. Lucas Paul Luchemba, for their invaluable guidance and support throughout my Master's dissertation. Their expertise, encouragement, and insightful feedback have been instrumental in shaping my research and propelling me towards this accomplishment. I am deeply grateful for their unwavering dedication, mentorship, and patience during challenging moments, which have profoundly enriched my academic journey and ultimately helped me reach this milestone.

Moreover, I am deeply indebted to all my colleagues in cohort 10 and my classmates Edna Kenneth and Restituta Ngowi, course instructors: Prof. Athanasia Matemu, Dr. Haikael Martin, Dr. Jofrey Raymond, Prof. Abraham Mpolya, Dr. Katherine Kreppal and the late Dr. Abrahaman Kipacha, the entire team from the School of Life Science and Bioengineering, as well as the BuSH. Their dedication and expertise have been invaluable throughout my studies.

Lastly, I extend my heartfelt appreciation to the esteemed management of the Nelson Mandela African Institution of Science and Technology for providing me with the opportunity to pursue my Master of Science in Human Nutrition and Dietetics. This academic endeavour has been an enlightening and invaluable experience.

DEDICATION

This work is dedicated to my beloved father, Dr. Alphonce Dotto Massaga; my cherished mother, Regina Salvatory Ngesela; my brothers, Deogratius Massaga and Dennis Massaga; my sister in heaven, Catherine Massaga; my amazing and supportive husband, Johnbosco Barnaba; and my kids, Johncaleb and Joanclarity.

TABLE OF CONTENTS

LIST OF TABLES

LIST OF FIGURES

LIST OF ABBREVIATION AND SYMBOLS

BBB	Blood-Brain Barrier
CDKs	Cyclin-Dependent Kinases
CNS	Central Nervous System
COX	Cyclooxygenase
EA	Ellagic Acid
EGFR	Epidermal Growth Factor Receptor
ETs	Ellagitannins
FDA	Food and Drug Administration
GPCRs	G Protein-Coupled Receptors
GPx	Glutathione Peroxidase
GRAS	Generally Recognized as Safe
GSH	Glutathione
GSTs	Glutathione S-Transferases
IQR	Interquartile Ranges
JNK	C-Jun N-Terminal Kinase
MAPK	Mitogen-Activated Protein Kinase
MAPK	Mitogen-Activated Protein Kinases
MCI	Mild Cognitive Impairment
MD	Molecular Dynamics
MGLT	Molecular Graphics Laboratory Tools
NSAIDs	Nonsteroidal Anti-Inflammatory Drugs
PDB	Protein Data Bank
PME	Particle Ewald
QS	Quorum Sensing
RCSB	Structural Bioinformatics
Rg	Radius of Gyration
RMSD	Root Mean Square Deviation
RMSF	Root Mean Square Fluctuation
RNS	Reactive Nitrogen Species
ROS	Reactive Oxygen Species
SASA	Solvent Accessible Surface Area
SOD	Superoxide Dismutase

WHO	World Health Organisation

CHAPTER ONE

INTRODUCTION

1.1 Background of the problem

The world's population is steadily growing (Gu *et al.*, 2021), with global life expectancy at birth rising from 66.8 years in 2000 to 73.3 years in 2019 (Cao *et al.*, 2023). This demographic shift has spurred growing interest in understanding and promoting healthy ageing strategies (Krivanek *et al.*, 2021). The World Health Organisation (WHO) defines healthy ageing as the process of developing and maintaining the functional ability that enables well-being in older age (Cesari *et al.*, 2022).

Biologically, ageing results from the cumulative effects of diverse molecular and cellular damage over time. This gradual accumulation leads to a decline in physical and mental capacity, an increased risk of disease and, ultimately, death (Okoro *et al.*, 2021). This age-related functional decline cannot be entirely attributed to a single mechanism or pathway (Franceschi *et al.*, 2018). Dementia, a general term encompassing impaired problem-solving, language difficulties, memory loss, and other cognitive abilities, affects approximately 45 million people worldwide.

This figure is projected to potentially double when mild cognitive impairment (MCI) is included (Schepens *et al.*, 2023). Moreover, projections estimate a tripling of this number to reach around 130 million by 2050 (Arvanitakis *et al.*, 2019; Schepens *et al.*, 2023). Beyond dementia, non-communicable diseases such as cardiovascular, diabetes, cancer and obesity further contribute to the global burden of mortality, with their share of all deaths increasing from 60.8% in 2000 to 73.6% in 2019 (WHO, 2017).

Modern medicine and nutritional evidence increasingly substantiate the efficacy of phytochemicals consumption in maintaining the body's functional ability, thereby contributing to healthy ageing (Park *et al.*, 2024; Ki *et al.*, 2024). Among phytochemicals, polyphenols are the most extensively studied, with over 8000 identified compounds (Alara *et al.*, 2021). However, a significant challenge remains due to the limited in vivo bioavailability of dietary polyphenols, as those with large molecular weight are often poorly absorbed in the gastrointestinal tract (Luca *et al.*, 2020; Scalbert *et al.*, 2002). Fortunately, gut microbiota plays a crucial role in overcoming this limitation.

Studies demonstrate that gut microbiota in the colon transforms polyphenols into bioactive metabolites, resulting in active and bioavailable metabolites with diverse functional capabilities (Luca *et al.*, 2020). This interaction is bi-directional as polyphenols provide sustenance for the gut microbiota, while the gut microbiota enhances the bioavailability of polyphenols (Makarewicz *et al.*, 2021). Notably, microbial-derived metabolites such as butyrate, tryptophan, urolithins, anthocyanins, equols and imidazole are gaining recognition as potential indicators for predicting individual health conditions and assessing drug effectiveness in vivo (Láng *et al.*, 2024).

Polyphenols, a diverse class of phytochemicals, are further categorised into phenolic acids, flavonoids, stilbenes, lignans and tannins (Prabhu *et al.*, 2021). While traditionally viewed by animal nutritionists as anti-nutritional due to the negative impact of tannins on protein digestibility (Bravo, 1998), recent advancements in gut microbiota research have shed new light on their beneficial interactions and effects (Cullen *et al.*, 2020). Explorations of the gut microbiota and the gut-brain axis have revealed key pathways influencing neurophysiology and behaviour.

These include neuroendocrinology (where microbiota influences neurogenesis), neuroimmune responses (where microbiota is crucial for microglial activation, the primary immune defence In the CNS (central nervous system), and neurotransmitters (microbiota acting as a pivotal role in methylation of the nerve cell). Additionally, microbial-derived metabolites (microbiota ferment raw materials such as polyphenols) yield active metabolites like Urolithin A, which perform various protective functions within the body. Collectively, these pathways highlight the influence of polyphenols and the gut microbiota on the host's neurophysiology and behaviour (Morais *et al.*, 2021).

Mounting evidence on host-microorganism interactions has fuelled increased interest in microbial metabolites (Hui *et al.*, 2021; Lee *et al.*, 2021). The metabolites include urolithins, which result from the gut microbial breakdown of ellagitannins (ETs) and ellagic acid (EA) and exhibit significant potential in delaying age-related diseases, including various cancers, cardiovascular diseases and chronic metabolic disorders (Boggia *et al.*, 2020; George *et al.*, 2023; Kuppusamy & Arumugam, 2023). Urolithin A, the most stable form of Urolithins, has garnered substantial attention due to recent studies highlighting its potential to positively affect brain ageing and combat neurodegenerative diseases (Bachli *et al.*, 2020; Djedjibegovic *et al.*, 2020; Gandhi *et al.*, 2024). Notably, Urolithin A has been proposed as a biomarker for

evaluating gut dysbiosis and tracking disease progression in individuals with Parkinson's disease (Nguyen *et al.*, 2023).

Integrating silico techniques into our exploration of Urolithin A allows us to uncover the complex molecular mechanisms at play, potentially revealing new therapeutic targets and clarifying previously misunderstood processes.

1.2 Statement of the problem

Despite the promising benefits of Urolithin A (Majdan & Bobrowska-Korczak, 2022), there remains a significant gap in understanding its precise mechanisms of action and overall efficacy in human health. Comprehensive insights into its molecular interactions, receptor binding affinities, and functional impacts on biomarkers associated with aging diseases are still needed. While traditional methods provide valuable insights, they often fail to reveal detailed molecular interactions. This gap presents a significant hurdle in developing targeted interventions for healthy ageing, particularly in the context of therapeutic product and nutraceutical development (Zhao *et al.*, 2023). This study utilized computational methods to address these gaps, including molecular docking and molecular dynamics simulations. These techniques provide valuable insights into how Urolithin A binds to and modulates key biological targets, revealing the underlying mechanisms responsible for its biological effects. Molecular docking studies elucidate the binding interactions of Urolithin A with specific targets. In contrast, molecular dynamics simulations offer insights into these interactions' stability and structural changes within a physiological context. The findings bridge the gap between experimental observations and mechanistic understanding, enhancing the knowledge of Urolithin A as a potential therapeutic agent for managing oxidative stress, inflammation and neurodegeneration. These results offer important implications for future clinical applications and targeted interventions, paving the way for more effective management of aging-related health conditions.

1.3 Rationale of the study

For comprehensive insights into molecular interactions, receptor binding affinities, and functional impacts on biomarkers associated with aging diseases are still needed. Traditional methods provide valuable insights, but fail to reveal detailed molecular interactions particularly in the context of therapeutic product and nutraceutical development (Zhao *et al.*, 2023). Revealing the underlying mechanisms responsible for its biological effects, the knowledge of Urolithin A as a potential therapeutic agent for managing oxidative stress, inflammation and

neurodegeneration grow and become potential for future treatment of complex non communicable diseases. These results offer important implications for future clinical applications and targeted interventions, paving the way for more effective management of aging-related health conditions.

1.4 Research objectives

1.4.1 General objective

This study aimed to explore the therapeutic potential of Urolithin A for healthy aging by employing molecular docking and dynamic simulations to elucidate its binding affinity and dynamic behaviour with target receptors.

1.4.2 Specific objectives

(i) To determine the nature of interactions between Urolithin A and selected receptors using molecular docking.

(ii) To assess the conformational stability of Urolithin A with the best candidate receptor by molecular dynamics simulation.

1.5 Research hypothesis

Null Hypothesis (H_0): Urolithin A does not exhibit significant binding affinity or conformational stability with target receptors associated with inflammation, oxidative stress and neurodegeneration, and thus lacks therapeutic potential for healthy ageing.

1.6 Significance of the study

By elucidating the intricate interactions of cellular processes through simulation, this study provides valuable insights into the fields of pharmacology, neuroscience and computational biology. It positions Urolithin A as a promising candidate for addressing various health conditions, including healthy ageing. Moreover, this study validates the effectiveness of computational tools such as AutoDock (Gaillard, 2018) and GROMACS (Kutzner *et al.*, 2022) in accurately predicting molecular interactions and dynamic behaviours. This validation not only enhances the robustness of these tools but also underscores their potential to advance therapeutic product discovery and molecular research, making them indispensable in future investigations.

1.7 Delineation of the study

This study contributes significantly to the broader understanding of Urolithin A and its potential applications in healthy ageing. By elucidating the precise molecular interactions of Urolithin A with various targets, this research provides a valuable blueprint for the development of nutraceutical products with targeted active sites. Understanding the molecular mechanisms underlying Urolithin A's health benefits will be instrumental in advancing personalised nutrition and precision medicine strategies for healthy ageing. This knowledge has the potential to inform the advancement of targeted interventions and significantly contribute to research and development efforts in this rapidly evolving field.

The present study had also limitations as explained as follows: While this study successfully demonstrated Urolithin A's binding affinity across multiple inflammation, oxidative, and neurodegenerative targets using molecular docking, molecular dynamics (MD) simulations were conducted only for the top-ranked complex p38 MAP kinase (PDB ID: 4DLI). This single-target focus, although justified statistically based on binding affinity and stability metrics, limits the depth of insight into Urolithin A's broader dynamic behaviour across other equally promising targets such as COX-2 (PDB ID: 5KIR) and Acetyl cholinesterase (PDB ID: 1B41).

The exclusion of these targets from MD simulation may constrain the interpretation of Urolithin A’s full multi-target therapeutic potential and raises the possibility of selection bias. Additionally, while computational tools like AutoDock and GROMACS provide robust predictive insights, they do not entirely replicate complex physiological environments. Further in vitro or in vivo validation is essential to support and expand upon these computational findings.

CHAPTER TWO

LITERATURE REVIEW

2.1 Overview of Urolithin A

Urolithin A arises as a natural dietary metabolite when the gut micro biome processes ellagitannin rich foods, a class of dietary polyphenols and hydrolysable tannins, along with ellagic acid, the hydrolysis product of ellagitannins (Verbeke *et al.*, 2015). Previously considered ant nutritional factors due to their association with tannins, recent scientific advancements have revealed that ellagitannins and ellagic acid can be converted into urolithins, including Urolithin A (D'Amico *et al.*, 2021), which exhibit diverse protective activities within the body (García-Villalba *et al.*, 2019). Urolithin A belongs to the class of organic compounds known as polycyclic aromatic compounds, with a chemical formula of $C_{13}H8O_4$ and a molar mass of 228.203 g/mol.

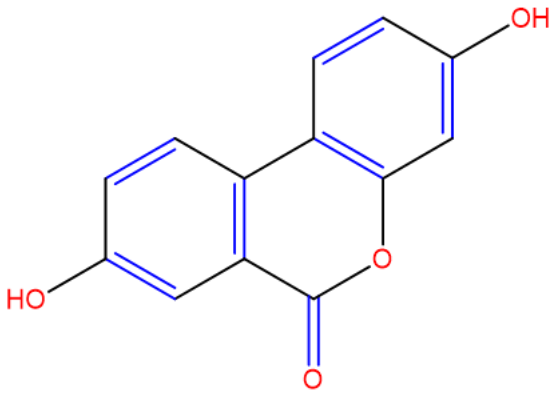

Figure 1: Chemical structure of Urolithin A

Foods rich in ellagitannins and ellagic acids, precursors to Urolithin A, were historically abundant in the diets of hunter-gatherer societies before the Industrial Revolution (Crozier *et al.*, 2010). Such foods include pomegranates, certain berries (including blackberries, cloudberries and raspberries), some types of nuts (such as chestnuts, pecans and walnuts), wine aged in wood, specific medicinal plants like Galla Chinensis, Nebulae Fructus and sea buckthorn leaf. While some of these foods are not commonly consumed in most African countries, including Tanzania (Okigbo & Anyaegbu, 2021; Olaoye *et al.*, 2020; Villalba *et al.*, 2019), recent research has identified guavas as a potential local source of ellagic acid and ellagitannins (Dhianawaty *et al.*, 2022). This discovery highlights the need for further research to identify additional commonly available foods high in Ellagitannins and Ellagic acid.

2.2 The biosynthesis of Urolithin A

Ellagitannins also Ellagic acid, despite their poor bioavailability in vivo, undergo a transformative process within the colon by intestinal microbes, yielding Urolithins with diverse biological activities (García-Villalba *et al.*, 2022a). Notably, the bioconversion of Urolithin A from Ellagitannins and Ellagic acid exhibits significant inter-individual variation (Romo-Vaquero *et al.*, 2015), leading to the classification of individuals based on their Urolithin-producing microbiota, termed "metabotype". These metabotypes range from Metabotype 0, which cannot produce any urolithin, to Metabotype A, which produces Urolithin A and Iso Urolithin A. They continue through Metabotype B, C and so on, with further sub-classifications based on the presence of additional urolithins like UroD to UroM-7 (Iglesias-Aguirre *et al.*, 2023). There are reportedly 13 urolithins and their conjugates, with Urolithin A and Urolithin B being the most stable. In contrast, others are considered intermediate compounds, which can be stabilised under various conditions (García-Villalba *et al.*, 2022b).

Factors influencing Urolithin A production include gut microbiota ecology, the presence of the correct metabotype, dietary intake of tannin-rich polyphenols and individual health status. Healthy individuals have a higher ability to produce Urolithin A compared to those under medication, which can disturb microbiota ecology. Digestive organ surgery and ageing, which diminish microbiota diversity and overall bodily function, also impact production. Therefore, Urolithin A supplementation becomes an appealing option for specific populations, particularly the elderly (Favari *et al.*, 2024; Singh *et al.*, 2022).

The microbial fermentation of Ellagitannins and Ellagic acid occurring in the colon generates Urolithin A. Studies reveal that only about 40% of individuals possess the correct microbiota to produce Urolithin A. The specific microbiota involved includes *Gordonibacter pamelaeae*, *Proteobaceria*, *Gordonibacter urolithinfaciens*, *Clostridium*, *Ellagibacteriso urolithinifaciens* *Bifidobacterium pseudocatenulatum*, *Eubacterium*, *Enteroccocus faecium* (García-Villalba *et al.*, 2020; Gaya *et al.*, 2018; Selma *et al.*, 2014). The conversion of Ellagitannins and Ellagic acid is facilitated by physiological pH and microbial enzymes within the anaerobic environment of the colon (Landete, 2011).

Urolithin A exhibits excellent bioavailability and a favourable safety profile in both animals and humans (Djedjibegovic *et al.*, 2020; Hasheminezhad *et al.*, 2022). Recent multi-centre clinical trials have confirmed the long-term safety and tolerability of oral administration of

Urolithin A, leading to its recognition as Generally Recognized as Safe (GRAS) by the Food and Drug Administration (FDA) for use in food products (Djedjibegovic *et al.*, 2020; Hasheminezhad *et al.*, 2022). Remarkably, Urolithin A can traverse the blood-brain barrier (BBB), facilitating targeted distribution within the central nervous system (CNS). This unique attribute positions Urolithin A as a promising candidate for neurological interventions (Djedjibegovic *et al.*, 2020; Hasheminezhad *et al.*, 2022).

2.3 Preclinical and clinical studies

Numerous preclinical studies have consistently demonstrated the positive effects of Urolithin A across various domains. Clinical trials involving middle-aged and older adults with mild cognitive impairment (MCI) have shown cognitive improvements following daily pomegranate juice consumption, which correlates with increased plasma concentration of Urolithin A (ClinicalTrials.gov Identifier: NCT02093130) (Siddarth *et al.*, 2020). Similarly, studies have linked taking walnuts and berries to enhanced mental function and good memory performance in older people (Chauhan & Chauhan, 2020; Miller *et al.*, 2018; Tow *et al.*, 2022).

Recent clinical trials further indicate that the administration of Urolithin A enhances the function of skeletal muscle and promotes mitochondrial health in middle-aged and older individuals. (ClinicalTrials.gov Identifier: NCT02655393, NCT03464500 and NCT03283462) (Faitg *et al.*, 2023; Singh *et al.*, 2022). Urolithin A also appears to be beneficial for skin health, potentially supporting collagen, reducing wrinkles and protecting against photoaging (ClinicalTrials.gov Identifier: NCTO5300984, NCT05300542 and NCT05473832) (D'Amico *et al.*, 2023).

A study that clustered individuals based on their metabotype observed inter-individual heterogeneity in improving cardiovascular risk indicators in overweight and obese individuals consuming pomegranate juice. The results showed that people with metabotype A, who can produce Urolithin A, are at a lower risk of cardiovascular disease and have reduced lipid levels in the body (González-Sarrías *et al.*, 2017). Urolithin A has also been shown to improve mitochondria and cellular health by activating mitophagy. In a groundbreaking human clinical study, oral administration of Urolithin A to a group of elderly individuals for two weeks revealed its beneficial effects on mitochondrial function (Andreux *et al.*, 2019). Furthermore, studies have shown that the prolonged consumption of ellagitannins by individuals with appropriate gut microbiota responsible for Urolithin A conversion may offer protection against inflammatory bowel diseases (IBDs) and colon cancer (Kujawska & Jodynis-Liebert, 2020).

Urolithin A has demonstrated a pancreatic protective effect in diabetic mice. A study aimed at understanding its impact on diabetes found that Urolithin A regulates autophagy, thereby contributing to pancreatic protection (Tuohetaerbaike *et al.*, 2020). Another study investigated Urolithin A's potential to counteract ageing due to its antioxidant, anti-inflammatory, and anti-apoptotic properties. Results indicated that Urolithin A activated the mTOR signalling pathway, which mitigated age-related decline in the brains of mice (Chen *et al.*, 2019).

In a separate mice model, researchers investigated the neuroprotective effect of Urolithin A in the brain of mice with Parkinson's disease. The research evaluated balance problems, nerve cell breakdown, harmful effects on fats and levels of synuclein, along with indicators of defence against oxidation, inflammation and cell death. In a study by Kujawska *et al.* (2020), Urolithin A administration resulted in a range of neuroprotective effects in a relevant model. Improved postural stability was observed, along with increased survival of neurons and defence against oxidative damage and α-synuclein aggregation.

There was also an increase in mitochondrial aldehyde dehydrogenase activity and maintenance of anti-apoptotic protein levels. These findings collectively indicate the potential of Urolithin A for neuroprotection. Moreover, Urolithin A exhibited anti-obesity effects and the ability to prevent metabolic dysfunction by enhancing adipose tissue heat production in a mice model without causing adverse effects, suggesting its potential for clinical application in humans (Echeverria *et al.*, 2021).

2.4 Mechanisms of action of Urolithin A and pharmacological activities

2.4.1 Mitophagy activation

Mitophagy, a specialised form of autophagy, is a crucial cellular process responsible for the selective removal of damaged and dysfunctional mitochondria for clearance, rejuvenation and regulation. This process ensures the biogenesis of new, robust mitochondria, thereby maintaining mitochondrial quality and control (Onishi *et al.*, 2021). The regulation of mitochondrial autophagy involves proteins such as Parkin and PINK1, with Urolithin A playing a crucial role in activating this pathway (Huang *et al.*, 2023; Quinn *et al.*, 2020). Urolithin A also activates the expression of glutathione S-transferases (GSTs), which are detoxifying enzymes involved in autophagy. It stimulates the Nrf2-ARE signalling pathway, which further triggers the expression of glutathione S-transferases (Hassanein *et al.*, 2020). As individuals age, defects in mitophagy can lead to degenerative illnesses such as Alzheimer's disease, cancer

and Parkinson’s disease. Consequently, Urolithin A emerges as a promising candidate for pharmacological therapy targeting these conditions.

2.4.2 Antioxidant potential

Oxidative stress arises from an imbalance between the free radicles and antioxidants in the body, exacerbating chronic diseases and conditions such as cancer, cardiovascular disorders and diabetes if left unchecked (Adwas *et al.*, 2019). Urolithin A, an effective antioxidant, can neutralize free radicals and mitigate their damaging effects on cells (Cásedas *et al.*, 2020). This antioxidant activity alleviates oxidative stress in muscle cells and protects cellular structures and functions, thereby promoting muscle health. Urolithin A also activates key antioxidant enzymes in the body, including superoxide dismutase (SOD) and glutathione peroxidase (GPx) (Kujawska *et al.*, 2019). These enzymes actively scavenge free radicals and peroxides within cells, further reducing oxidative stress and promoting muscle health.

Additionally, Urolithin A stimulates the production of antioxidant molecules such as glutathione (GSH) and glutathione S-transferase (Zhao *et al.*, 2023). Its antioxidant properties enable it to eliminate free radicles, inhibit lipid peroxidation, and modulate intercellular reactive oxygen species (ROS) and reactive nitrogen species (RNS). Furthermore, Urolithin A inhibits oxidizing enzymes like tyrosine and monoamine oxidase, playing a crucial role in regulating oxidative stress and maintaining muscle cells' health.

Due to its neuroprotective effects, including the reduction of brain oedema, neuronal apoptosis, neurobehavioral impairments and the protection of the blood-brain barrier, Urolithin A shows promise as a treatment for traumatic brain injury. The potential mechanism for Urolithin A's neuroprotective effects against traumatic brain damage involves the suppression of the PI3K/Akt/mTOR and Akt/IKK/NFκB signalling pathways, which can result in decreased neuroinflammation and increased autophagy (Gong *et al.*, 2022).

2.4.3 Anti-inflammatory activities

Inflammation is a natural response of the body to combat foreign matter such as diseases, microbes, infections, and injuries (Bai *et al.*, 2021). However, chronic inflammation can become life-threatening, leading to conditions as asthma, cancer, cardiovascular diseases and neurodegenerative disorders, depending on the site of inflammation (Huang *et al.*, 2021). Free radicles in the body can also trigger inflammation. Initially, nonsteroidal anti-inflammatory drugs (NSAIDs) and selective COX-2 inhibitors were developed to reduce gastric

complications (Bindu *et al.*, 2020). However, COX-2 inhibitors like celecoxib and rofecoxib were linked to increased cardiovascular risks, leading to Vioxx's withdrawal from the market (Rogers *et al.*, 2020).

Urolithin A exhibits significant anti-inflammatory properties by neutralising free radicals, which are a source of inflammation. It also inhibits specific enzymes involved in inflammation, such as cyclooxygenase (COX). The COX enzymes, including COX-1 and COX-2, are crucial for the synthesis of prostaglandins, prostacyclins, and thromboxanes (Faki & Er, 2021). By blocking these enzymes, Urolithin A effectively reduces inflammation and the associated pain. The NF-κB pathway plays a pivotal role in regulating inflammatory reactions. Urolithin A inhibits NF-κB activation, thereby reducing inflammation and muscle damage, as well as promoting muscle repair and overall muscle health.

Additionally, Urolithin A inhibits the NF-κB/STAT1 axis by deactivating TLR3/TRIF signalling, significantly attenuating chronic inflammation associated with ageing. It demonstrates significant anti-inflammatory effects by inhibiting NO production, iNOS and COX-2 expression while modulating pro-inflammatory and anti-inflammatory cytokine levels. Specifically, Urolithin A targets the NLRP3 inflammasome, thereby reducing its expression and activity (Gupta *et al.*, 2021).

2.4.4 Anti-microbial properties

Microbes, such as bacteria, protozoa, fungi and even viruses, which are naturally found in the environment and the human body, can be either beneficial or harmful (Zhang *et al.*, 2023). In a rat model, Urolithin A demonstrated the ability to control the development of bacteria before and after chemically induced inflammation. Urolithin A also reduced the levels of AHLs produced by the enteropathogens by inhibiting quorum sensing (QS), processes by up to 40% (Nazzaro *et al.*, 2013). Quorum sensing is a microbial communication method that enables microorganisms to coordinate infection-related processes such as motility and virulence. Thus, Urolithin A exhibits antimicrobial activity by disrupting these QS mechanisms.

Given the increasing recognition of gut metabolites in human health, Urolithin A emerges as a promising therapeutic approach. Metabolite-based treatments, compared to microbiome-based treatments, overcome limitations such as colonization resistance and inter-individual variations in microbial composition, potentially offering enhanced efficacy downstream of the

microbiome (Suez & Elinav, 2017). These attributes collectively underscore the potential of Urolithin A in developing functional foods or therapeutic products.

2.4.5 Urolithin A in inhibiting protein glycation

Glycation refers to the non-enzymatic binding of sugar to lipids, proteins, or DNA (Rehman *et al.*, 2022). It serves as a crucial biomarker for diabetes, various other conditions, and ageing. Elevated protein glycation, a consequence of hyperglycaemia, significantly contributes to cardiovascular diseases, diabetes and Alzheimer's disease (Rungratanawanich *et al.*, 2021). Urolithin A exhibits anti-glycemic properties independent of antioxidant activity, potentially playing a crucial role in stress management and the maintenance of muscle cell health (Raina *et al.*, 2023).

2.4.6 Regulation of apoptosis and cell cycle

Research indicates that Urolithin A can regulate the cell cycle and induce apoptosis (Mohammed *et al.*, 2020). It influences cell cycle-related protein kinase complexes, such as cyclin-dependent kinases (CDKs) and cyclins (El-Wetidy *et al.*, 2021). Urolithin A inhibits CDK activity and decreases the production of cell cycle proteins like cyclin D1, leading to cell cycle arrest in the G1 phase (Okumura, 2021). Furthermore, Urolithin A can regulate the cell cycle by increasing the amounts of cell cycle inhibitory proteins such as p21 and p27 (Berdowska *et al.*, 2021). Studies have shown that urolithin A increases the Bax/Bcl-2 ratio, resulting in mitochondrial membrane potential loss, cytochrome c release and activation of caspase cascade, all of which contribute to cell apoptosis (El-Wetidy *et al.*, 2021). Urolithin A also stimulates the JNK (c-Jun N-terminal kinase) and p38 MAPK (mitogen-activated protein kinase) signalling pathways, further promoting apoptosis.

2.4.7 Metabolic regulation

Urolithin A exhibits metabolic regulatory properties through its interaction with key signalling pathways. It can activate the AMPK signalling pathway, a central regulator of energy metabolism. The AMPK activation promotes fatty acid oxidation and insulin sensitivity while simultaneously suppressing fatty acid synthesis and gluconeogenesis (Lin *et al.*, 2020). Urolithin A also regulates the activity of PPARγ, a transcription factor governing adipocyte development, glucose metabolism, and cholesterol homeostasis. Studies have shown that Urolithin A upregulates PPARγ expression and its target gene transcription, leading to

increased fatty acid oxidation, improved insulin sensitivity, and reduced cholesterol production and absorption (Toney *et al.*, 2021).

2.5 Molecular dynamics

Molecular dynamics (MD) simulation involves understanding the characteristics of macromolecules by emulating atomic behaviour using predefined potential energy. During an MD simulation, particles interact within specified intervals, generating a trajectory that elucidates the dynamic properties of the system (Gartner III & Jayaraman, 2019). This study begins by exploring the fundamental elements of system dynamics. To properly conduct a molecular dynamics simulation on a specific system, it is essential to have microscopic-level data, including atomic velocity and position based on a specific potential energy function, as shown in Fig. 2. This energy function facilitates the determination of forces acting upon each atom concerning its position relative to others. Typically, classical mechanics govern the microscopic behaviour of systems, describing how forces influence atomic motions according to Newton's laws (Belubbi & Martis, 2017; Bernath, 2020).

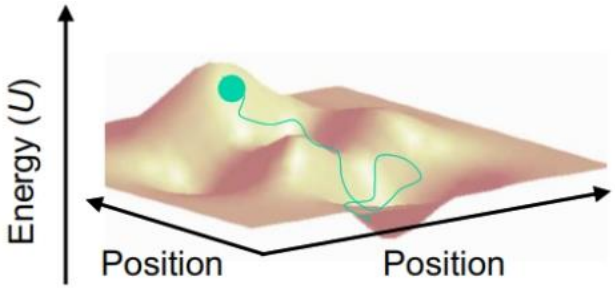

Figure 2: System energy function and position of its atoms

Computation of force is deriving the potential that interacts, denoted as V(R). Equation 1 provides the force applied to each unique particle in the system (Bader, 1998).

$$F_i = m_i a_i = m_i \frac{d^2 r_i}{dt^2} = -\nabla V(R) \tag{1}$$

The Fi value, which is determined by vector summation, is the total force applied to the i^{th} atoms in the system. Furthermore, each atom's mass is represented by *mi*, while its acceleration is represented by *ai* (Alturki *et al.*, 2020). The positions of individual atoms are found by merging information about the mass of the atom and force over a sequence of discrete time steps (usually spanning from 1 to 10 femtoseconds) (National Academies of Sciences *et al.*, 2020). Beginning locations and velocities are usually well-defined in the input data file, and forces are obtained from measurements of potential energy (Van de Vijver & Zádor, 2020).

The Maxwell-Boltzmann distribution is used to assign velocities at a specific temperature (often set at 300 Kelvin in most biological systems), while preliminary coordinates at t = 0 are extrapolated from experimental data (Roduner & Krüger, 2022).

2.5.1 Analytical approaches in molecular dynamics simulations

Molecular dynamics (MD) simulations provide atomic-level insights into the behavior and stability of protein-ligand complexes over time. The trajectory data generated from MD simulations is analyzed using several quantitative parameters. Among the most widely employed are Root Mean Square Deviation (RMSD), Root Mean Square Fluctuation (RMSF) and Radius of Gyration (Rg, and Solvent Accessible Surface Area (SASA). Each of these parameters reveals distinct but complementary structural and dynamic aspects of biomolecules, particularly in the context of drug binding and protein conformational dynamics.

The RMSD measures the average positional deviation of atoms (commonly backbone atoms) of a protein or complex concerning a reference structure (usually the initial conformation). It is a global measure of structural stability. It indicates how much a protein or protein-ligand complex deviates from its original conformation over time. A low and stable RMSD suggests that the system is equilibrated and structurally stable (Yun & Guy, 2011). It is used to monitor structural equilibration by comparing the apo and ligand-bound forms, thereby assessing the structural perturbation upon ligand binding. When a plateau is observed, it indicates that a stable structure has formed. An increasing trend suggests a structural deviation, while large fluctuations may indicate instability or flexible domains. The RMSD has some limitations; it does not capture local structural rearrangements, it is sensitive to domain movements and alignment errors (Amadei *et al.*, 1993; Hollingsworth & Dror, 2018).

The RMSF quantifies the average deviation of each residue or atom over time from its mean position. It provides residue-level flexibility, allowing identification of stable and dynamic regions within the protein. It is especially valuable for analyzing loop regions and binding site residues; usually used to identify flexible loops or disordered regions, evaluate stability of binding site residues also to compare dynamics of bound vs. unbound proteins (Weinhäupl *et al.*, 2018). During interpretation when a Low RMSF is observed indicates a stable with ordered regions (e.g., alpha-helices, beta-sheets), and when a high RMSF is observed indicates flexible or disordered regions (e.g., terminal loops, binding loops) (Lindorff-Larsen *et al.*, 2010).

The MSF is limited in its ability to capture rapid, time-resolved changes because it provides an average measure of atomic motion over a specified time window or set of structures. By

averaging, it can mask transient fluctuations and conformational changes that occur on shorter timescales; also RMSF is not an effective measure for assessing global protein stability because it focuses on the local flexibility of individual residues rather than the overall structural integrity of the protein. While RMSF can reveal regions of high or low flexibility within a protein, it doesn't directly indicate whether the protein as a whole is stable or prone to unfolding or denaturation (Pradhan, 2017).

The Radius of Gyration represents the root mean square distance of all atoms from the protein's center of mass. It reflects the overall compactness or folding state of a protein. It is a key indicator of structural integrity during ligand binding or environmental stress. It is used to assess conformational folding/unfolding, to compare compactness between bound and unbound forms, and to detect protein collapse or unfolding events (Sailah *et al.*, 2021). In interpretation a stable Rg is when compact and structurally intact protein is seen compared to the apo, when the Rg is decreasing implies protein compaction or folding, and increasing Rg is possible unfolding or expansion. The radius of gyration, while a useful concept in mechanics, has limitations. It primarily applies to objects with uniform mass distribution and a fixed axis of rotation (Abramowicz *et al.*, 1993). It doesn't accurately represent the rotational inertia of objects with complex shapes or varying mass densities, nor does it account for changing axes of rotation. Furthermore, it doesn't directly address situations where the mass distribution is non-uniform or the axis of rotation is not fixed.

The SASA calculates the surface area of a biomolecule that is accessible to a solvent, typically water. It is useful in assessing the folding state of proteins and the exposure of hydrophobic or hydrophilic regions, which may influence ligand binding (Ausaf-Ali *et al.*, 2014). Together, these parameters provide a comprehensive understanding of how ligand binding influences protein structure and dynamics, helping to predict the efficacy and stability of the ligand–receptor complex in a simulated biological environment. Solvent accessible surface area (SASA) calculations, while useful, have limitations in accurately representing protein-solvent interactions and can be computationally intensive for certain applications. Specifically, they struggle with capturing the full complexity of protein-solvent-protein interactions and can be inaccurate when applied to unfolded protein states (Kim & Na, 2022).

2.6 Energy minimisation

The preliminary setup for molecular dynamic simulations is obtained from various experimental techniques, such as electron diffraction, neutron and X-ray, as well as Raman,

neutron spectroscopy, infrared and NMR (Bon *et al.*, 2020). Molecular frameworks often face issues of instability and frequent collisions, which calls for energy minimization to achieve stability (Shi & McHugh, 2023). This involves the strategic arrangement of atoms in space to ensure that the net force between atoms and each atom diminishes towards zero. Additionally, it's essential to guarantee that the position on the energy-possessed surface aligns with a stationary point, as per the chemical bond in a theoretical model (Broad *et al.*, 2021).

2.7 Force fields

This mathematical construct describes the relationship between the spatial arrangement and constituent particles of a system's energy (Frishman & Ronceray, 2020). It encompasses an analytical representation of potential energy between atoms interatomic, denoted as U (r1, r2,..., rN), along with numerous associated constraints (Hurley *et al.*, 2005). Fitting experimental data typically derives these parameters from techniques such as neutron, X-ray, electron diffraction and NMR spectroscopy to ab initio or semi-empirical quantum mechanical calculations. Equation 2 provides an exemplary expression for a typical force field (Allinger, 2010).

$$U = \sum_{\text{bonds}} \frac{1}{2}k_b(r - r_0)^2 + \sum_{\text{angles}} \frac{1}{2}k_a(\theta - \theta_0)^2 + \sum_{\text{torsions}} \frac{V_n}{2}[1 + \cos(n\phi - \delta)] + \sum_{\text{improper}} V_{imp} + \sum_{\text{LJ}} 4\epsilon_{ij}\left(\frac{\sigma_{ij}^{12}}{r_{ij}^{12}} - \frac{\sigma_{ij}^{6}}{r_{ij}^{6}}\right) + \sum_{\text{elec}} \frac{q_i q_j}{r_{ij}} \quad (2)$$

From the above equation, the four first terms elucidate localized impacts or intramolecular on the overall energy, encompassing improper torsions, dihedral, bond stretching and angle bending. Conversely, the last two delineate repulsive interactions: The Coulombic interactions and van der Waals forces (represented here by a 12–6 Lennard–Jones potential).

Force fields typically include practical terms, for example, Coulombic, Lennard–Jones and harmonic vibration, along with model features defining these functions. Molecular dynamic simulations offer a variety of force fields some are: The AMBER, CHARMM27, GROMOS and OPLS. Therefore, selecting a force field for MD simulations depends on the system under investigation.

2.8 Integrating the equation of motion

Molecular mechanics simulations use force fields to define the interactions between atoms within a system. By calculating these forces, the positions and velocities of individual particles can be determined. A minimal time step Δt of approximately 1 femtosecond (fs) is typically

employed to ensure accuracy. However, extending simulation time can pose challenges in maintaining energy conservation. Several numerical integration algorithms have been developed to solve the equations of motion in molecular dynamics simulations, including Beeman's algorithm, Leap-frog algorithm, Symplectic reversible integrators, Velocity Verlet and Verlet's algorithm. Among these, Verlet's algorithm remains the most employed method. It leverages Taylor series expansions derived from particle coordinates at times $t \pm \Delta t$, where Δt represents the chosen time step.

CHAPTER THREE

MATERIALS AND METHODS

3.1 Materials

The software utilised in molecular docking experiments includes AutoDock Vina for running docking processes, Molecular Graphics Laboratory Tools (MGLT) for molecular visualisation, analysis and manipulation and Open Babel for converting input structures into the desired output structures. The PyMOL, Chimera, and Discovery Studio were employed for visualization and analysis. In molecular dynamics simulations, SWISSPARA and GROMACS were the primary tools (Irrgang *et al.*, 2022). The CHARMM force field was selected for its compatibility with protein systems.

3.2 Methods and steps used to determine the nature of interactions with selected receptors of Urolithin A

3.2.1 Protein selection and preparation

Proteins were selected based on their target for nutraceutical development in healthy ageing. The crystal structures for the selected receptors were retrieved from the Protein Data Bank (PDB) hosted by the Research Collaborators for Structural Bioinformatics (RCSB) (Goodsell *et al.*, 2020). A series of cleaning steps was performed using Chimera software to prepare the structures for docking simulations (Kim *et al.*, 2016). This involved removing solvent molecules, non-complex ions and any ligands already bound to the receptor. The Dunbrack rotamer library completed the missing side chains to achieve complete initial structures (Halgren, 1996). Subsequently, hydrogen atoms were added and Kollman charges (Gasteiger & Marsili, 1980) were assigned to the structures, reflecting a physiological pH of 7.4.

Finally, the prepared protein structures were converted to the PDBQT format for compatibility with Autodock Vina docking software (Trott & Olson, 2010). The following proteins were chosen for docking simulations due to their critical roles in anti-oxidation, anti-inflammation and neuro-protection.

(i) Human topoisomerase IIα ATPase/AMP-PNP (protein data bank ID: 1ZXM)

Human topoisomerase IIα, an enzyme crucial in DNA metabolism, plays a significant role in untangling and rearranging DNA strands during vital cellular activities such as coding and

transcription (Atkin *et al.*, 2019). Given its involvement in DNA metabolism and maintenance, it holds potential implications for various ageing-related processes (Nitiss, 2009).

(ii) Human cytochrome P450 CYP2C9 (protein data bank ID: 1OG5)

Human Cytochrome P450 CYP2C9, identified by its Protein Data Bank ID 1OG5, is primarily situated in the liver, where it serves a crucial role in detoxifying a wide array of drugs and xenobiotics (Zhao *et al.*, 2021). This enzyme is responsible for catalysing the oxidation of numerous substrates, including non-steroidal anti-inflammatory drugs (NSAIDs), anticoagulants like warfarin, and antiepileptic drugs, among others (Daly *et al.*, 2017).

Given its significance as a major therapeutic-metabolising enzyme in the liver, CYP2C9 likely contributes to maintaining overall health and well-being by regulating the metabolism of various medications and xenobiotics (Hadia *et al.*, 2024). Its activity is presumed to influence the efficacy and safety of therapeutic compounds commonly prescribed to older adults for managing chronic conditions associated with ageing, such as cardiovascular disease, diabetes, and arthritis (Lenoir *et al.*, 2021).

(iii) Epidermal growth factor receptor tyrosine kinase domain with 4-anilinoquinazoline inhibitor erlotinib (protein data bank ID: 1M17)

The Epidermal Growth Factor Receptor (EGFR) Tyrosine Kinase Domain, when targeted with 4-anilinoquinazoline inhibitors like Erlotinib, holds considerable significance in cancer therapy (Yang *et al.*, 2022). Erlotinib, a 4-anilinoquinazoline inhibitor, operates by binding to the tyrosine kinase domain of EGFR, effectively obstructing the ATP-binding site. This action inhibits the receptor from phosphorylating downstream signalling molecules, thereby impeding the growth and proliferation of cancer cells (Mohammed *et al.*, 2023). Consequently, Erlotinib's efficacy in decelerating or halting cancer cell growth, leading to tumour regression and improved patient outcomes, underscores the potential of targeted therapies to address specific cellular dysfunctions.

(iv) Kinase P38/SB203580 complex (protein data bank ID: 1A9U) and p38 MAP kinase in complex with RL87 (protein data bank ID: 4DLI)

The p38 MAP kinase (Mitogen-Activated Protein Kinase) is a type of protein kinase that plays a critical role in cellular signalling pathways involved in various physiological processes (Yue & López, 2020). It is stimulated in reply to a variety of extracellular stimuli, including pro-

inflammatory cytokines (such as TNF-α and IL-1β), environmental stressors (such as heat shock, osmotic shock, and UV radiation) and cellular damage (Mai *et al.*, 2020). The SB203580 is a small-molecule compound that inhibits p38 kinase. It binds to the ATP-binding site of p38 kinase, thereby inhibiting its enzymatic activity (Haller *et al.*, 2020).

(v) Vioxx bound to Human COX-2 (protein data bank ID: 5KIR)

Vioxx is a nonsteroidal anti-inflammatory drug (NSAID) that was used to relieve pain and inflammation, particularly in conditions like osteoarthritis and rheumatoid arthritis (Bindu *et al.*, 2020). It belongs to a class of drugs known as selective COX-2 inhibitors. The Cyclooxygenase-2 (COX-2): The COX-2 is an enzyme involved in the production of prostaglandins, which are lipid mediators that play a role in inflammation, pain and fever (Ju *et al.*, 2022).

(vi) Solution structure of Alzheimer's disease amyloid beta-peptide (1-42) (protein data bank ID: 1IYT)

The Amyloid Beta peptide is a small protein fragment that plays a central role in the pathogenesis of Alzheimer's disease (Roda *et al.*, 2022). The Aβ peptides are produced through the sequential cleavage of a larger protein called the amyloid precursor protein. Their abnormal aggregation and accumulation in the brain are hallmark features of Alzheimer’s disease (Delport & Hewer, 2022).

(vii) Acetyl cholinesterase (protein data bank ID: 1B41)

Acetyl cholinesterase is predominantly located in nerve cells and red blood cells, where its primary role is to catalyse the hydrolysis of the neurotransmitter acetylcholine into choline and acetate following the transmission of a nerve impulse (Walczak-Nowicka & Herbet, 2021). In healthy ageing, the role of acetyl cholinesterase remains crucial, primarily in maintaining proper cholinergic neurotransmission (Silman, 2021).

(viii) Neurotensin receptor (protein data bank ID: 1GQR)

Neurotensin receptors belong to a class of G protein-coupled receptors (GPCRs), which are stimulated by the neuropeptide neurotensin (Zhang *et al.*, 2021). Neurotensin, a 13-amino acid peptide, functions as a neurotransmitter and a hormone in the central nervous system and the gastrointestinal tract (Mishra & Mohanty, 2023).

(ix) Human dipeptidyl peptidase-4 (protein data bank ID: 4EY7)

An enzyme belonging to the serine protease family (Chitadze *et al.*, 2021). As a cell surface protein, DPP-4 regulates both glucose metabolism and immune response.

3.2.2 Ligand (Urolithin A) preparation

Urolithin A in Structure Data Files format was retrieved from the PubChem database (Kim *et al.*, 2016). Gasteiger charges were added to the ligand, followed by energy minimization using Merck Molecular Force Field (MMFF94) (Gasteiger *et al.*, 2021) to ensure conformation stability before docking studies in Avogadro. Subsequently, the optimized structure was converted to PDBQT format, rendering it ready for molecular docking.

3.2.3 Molecular docking simulations

Molecular docking was performed using AutoDock Vina to predict the binding affinity and interaction mode between Urolithin A and selected protein targets. For each receptor-ligand pair, 20 docking runs were executed to generate multiple binding poses and ensure sampling of diverse conformations. The grid box was carefully defined to encompass the entire active or catalytic site of each receptor, with dimensions set at 30 × 30 × 30 Å in the X, Y and Z axes, respectively. The grid box was centred on the active site residues identified from the co-crystallized ligand or literature-reported binding pocket, with a spacing of 0.375 Å, which is standard for AutoDock Vina. This configuration allowed for accurate and consistent docking results across all target proteins. The docking results were ranked based on binding affinity scores, and the top-scoring poses were selected for further analysis and visualization using Discovery Studio and UCSF Chimera.

3.3 Methods used to assess the conformational stability of Urolithin A with the best candidate receptor

3.3.1 Molecular dynamics simulation ligand preparation

For molecular dynamics simulations, the protein-ligand complex with the lower binding affinity value, indicative of stronger binding from the molecular docking results, was selected as the input structure. Ligand parameters were generated using the Swisparam server, ensuring compatibility with the CHARMM force field (Zarougui *et al.*, 2023).

3.3.2 Application of GROMACS

The Molecular Dynamics simulations were performed using the GROMACS 2020 software package, employing the CHARMM force field to define protein atoms. The ligand-protein complex system was solvated with the TIP3P water model within a cubic simulation box. To maintain system neutrality, counter ions were added. Subsequently, energy minimization was conducted for 5000 steps using the steepest descent algorithm with a convergence tolerance of Fmax < 1000 kJ/mol. Following energy minimisation, a two-step equilibration process was implemented. The first equilibration step employed the NVT ensemble (Constant Number of Particles, Volume, and Temperature) for 100 picoseconds.

During this phase, the Berendsen thermostat maintained a constant temperature of 300 K while the pressure was maintained at 1 bar. Afterward, equilibration, the molecular dynamic simulation run was executed for 100 nanoseconds in the NPT ensemble (Constant Number of Particles, Pressure and Temperature). The Parrinello-Rahman barostat ensured a constant pressure of 1 bar at 300 Kelvin, achieved through temperature coupling. The Particle Ewald (PME) method was applied to treat long-range electrostatic interactions, algorithm used was LINCS so as to constrain covalent bonds. The 2 femtoseconds (fs) were used for all calculations as time step. Throughout simulation the pressure, density and energy were monitored.

3.4 Analysis

Although this study did not involve classical hypothesis testing, the interpretation of the quantitative results followed structured analytical criteria based on established computational and molecular modelling protocols. Binding affinities obtained through AutoDock Vina were interpreted using standard thresholds, where more negative Gibbs free energy values indicate stronger ligand–receptor binding. The nature of these interactions such as hydrogen bonding, van der Waals forces, π–π stacking, and electrostatic interactions, was examined through Discovery Studio and Chimera visualizations, enabling qualitative and quantitative insights into binding stability and specificity.

Specifically, the study employed descriptive statistical techniques to interpret and visualize the distribution and variation of binding affinities and dynamic simulation outputs. For the molecular docking results, a boxplot (Fig. 13) was generated to depict the distribution of Urolithin A’s binding affinities across multiple target proteins. This visualization included

interquartile ranges (IQR), median values (as central tendency), whiskers (representing 1.5× IQR), and identified outliers using standard statistical rules. These elements were used to compare binding energy ranges and determine the variability and strength of ligand–receptor interactions.

For molecular dynamics (MD) simulations, a range of structural and thermodynamic parameters were computed to assess the conformational stability of the Urolithin A–protein complex across a 100-nanosecond trajectory. These included Root Mean Square Deviation (RMSD) to evaluate overall structural fluctuations, Root Mean Square Fluctuation (RMSF) to measure residue-level flexibility, Radius of Gyration (Rg) for compactness assessment, and Solvent Accessible Surface Area (SASA) to determine surface exposure changes upon binding. Hydrogen bond counts were tracked over time to assess the persistence and quality of molecular interactions. The statistical plots and data analyses were generated using built-in functions from GROMACS 2020, an open-source molecular dynamics package, as well as GraphPad Prism and Excel for post-processing and visualizing the boxplots and distribution curves.

These data interpretation methods ensured that the computational findings were not only technically sound but also scientifically meaningful in evaluating the therapeutic potential of Urolithin A.

CHAPTER FOUR

RESULTS AND DISCUSSION

4.1 Results

The Chapter presents the findings obtained from docking analyses investigating the interactions between Urolithin A and the selected receptors. It encompasses insights into the binding energy and the specific binding interactions between Urolithin A and the residues of the target protein. The chapter also delves into the conformational stability of Urolithin A when bound to the most promising candidate receptor, shedding light on the intricate molecular mechanisms at play.

4.1.1 Nature of interactions with Urolithin A selected receptors

Docking simulations were carried out using AutoDock Vina, with 20 runs performed per receptor-ligand pair to obtain a range of potential binding poses. The docking grid box was uniformly defined across all proteins to cover the active site, with dimensions of 30 Å × 30 Å × 30 Å, and spacing of 0.375 Å. This ensured thorough sampling of the ligand's conformational space within the binding pocket. The binding affinities obtained from these docking runs were then statistically analyzed and presented using a boxplot (Fig. 13), which summarizes the distribution of scores across all target receptors. Top-scoring binding poses were further examined for key molecular interactions such as hydrogen bonding, van der Waals contacts, and π–π stacking using Discovery Studio and UCSF Chimera.

The interactions between the ligand, Urolithin A, and the chosen target receptors, along with their respective binding free energies, were thoroughly examined using molecular docking techniques. These results are briefly outlined in Fig. 3-11 and summarised in Table 1. Notably, a diverse range of binding energy ranging from ¯5.5 to ¯10.1 kcal/mol was observed across the selected receptors, as depicted in Table 1. Particularly noteworthy is the observation that Human p38 MAP kinase in complex with RL87 (Protein Data Bank ID: 4DLI) exhibited the strongest binding energy of ¯10.1 kcal/mol compared to other receptors under investigation.

(i) Human p38 MAP kinase in complex with RL87 (protein data bank ID: 4DLI)

Figure 3 illustrates the binding profile of Human p38 MAP kinase in complex with RL87 (PDB ID: 4DLI), showcasing various interactions exhibited by Urolithin A. Firstly, Urolithin A engages in van der Waals interactions with SER^{293}, GLU^{192}, ALA^{255}, SER^{252}, LYS^{249} and

ASP[294]. Secondly, it forms the PI-interaction with TRP[197], ASN[196]. Lastly, hydrogen bond interactions are observed between Urolithin A and ASP[292], LEU[195] and GLU[198]. These diverse interactions collectively contribute to the robust binding affinity of Human p38 MAP kinase in complex with RL87 (PDB ID: 4DLI).

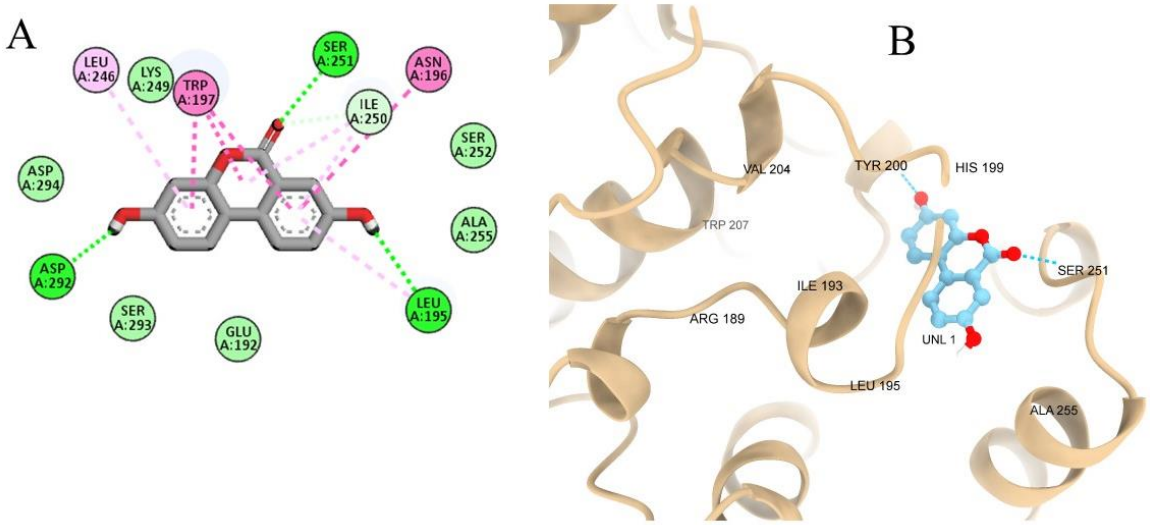

Figure 3: Interaction properties between Urolithin A and Human p38 MAP kinase in complex with RL87 (PDB ID: 4DLI) using Discovery Studio Visualizer (A) and Chimera (B)

(ii) Kinase P38/SB203580 complex (protein data bank ID: 1A9U)

Kinase P38/SB203580 complex having the binding energy of ¯6.8 kcal/mol exhibited a varied interaction profile with Urolithin A, as depicted in Fig. 4. The interaction profile includes a diverse array of interactions, including van der Waals interactions with LEU[74], LEU[171], ILE[84], ASP[168], TYR[35] and PHE[169], Pi interactions with GLU[71], LYS[53], ARG[173] and PI-alkyl interactions with LEU[75], ALA[172].

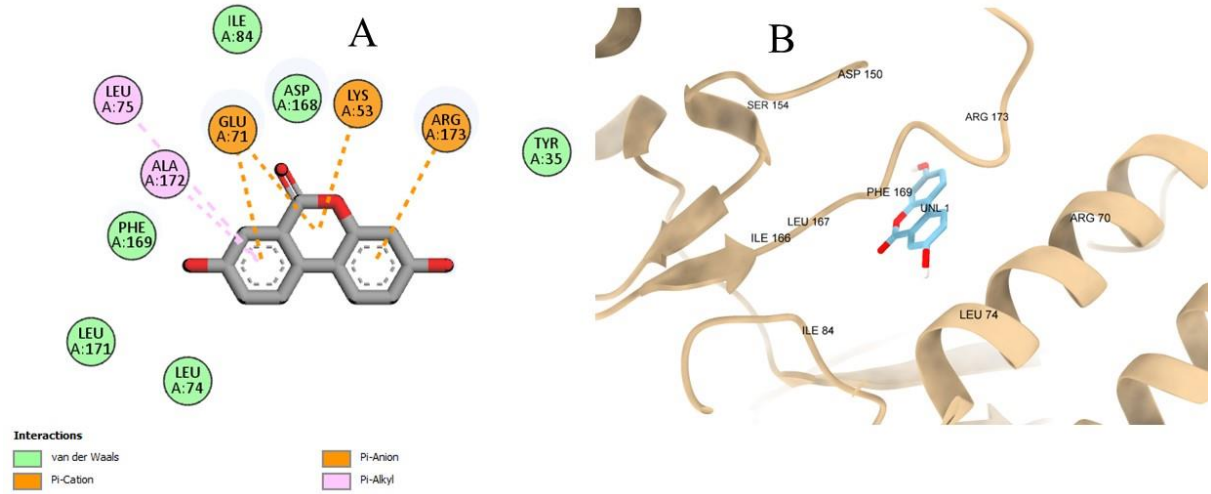

Figure 4: Interaction properties between Urolithin A and Kinase P38/SB203580 complex (PDB ID: 1A9U) using Discovery Studio Visualizer (A) and Chimera (B)

(iii) Vioxx Bound to Human COX-2 (protein data bank ID: 5KIR)

Figure 5 illustrates the binding profile of Vioxx Bound to Human COX-2 (PDB ID: 5KIR) with Urolithin A. The binding affinity of Urolithin A to the Vioxx Bound to Human COX-2 (PDB ID: 5KIR) receptor was ¯8.6 kcal/mol. This interaction involved key amino acid residues contributing to the subsequent interactions, including van der Waals interactions with LEU^{391}, PHE^{200}, LEU^{390}, GLN^{203}, TRP^{387}, THR^{206}, PHE^{210}, ASN^{382} and HIS^{386}.

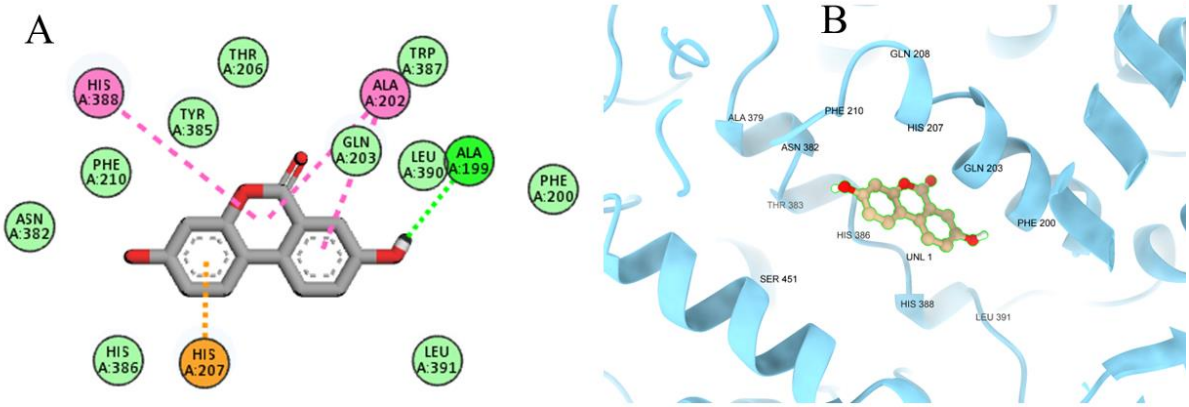

Figure 5: Interaction properties between Urolithin A and Vioxx Bound to Human COX-2 (PDB ID: 5KIR) using Discovery Studio Visualizer (A) and Chimera (B)

(iv) Human topoisomerase IIα ATPase/AMP-PNP (protein data bank ID: 1ZXM)

The binding profile of Human Topo IIa ATPase/AMP-PNP with PDB ID (1ZXM) against Urolithin A is shown in Fig. 6. The binding affinity of Urolithin A in Human Topo IIa ATPase/AMP-PNP with PDB ID (1ZXM) receptor was calculated to be ¯7.4 kcal/mol. The binding energy is attributed to various amino acids, each contributing through different types

of interactions: Van der Waals with LYS[205], ASP[37], ALA[209], GLU[38], TYR[36], TYR[216] and LEU[234]; Pi-sigma with VAL[212], Pi-Alkyl with VAL[205]; and H-bond interactions with LEU[229], ASN[232] and ASN[230].

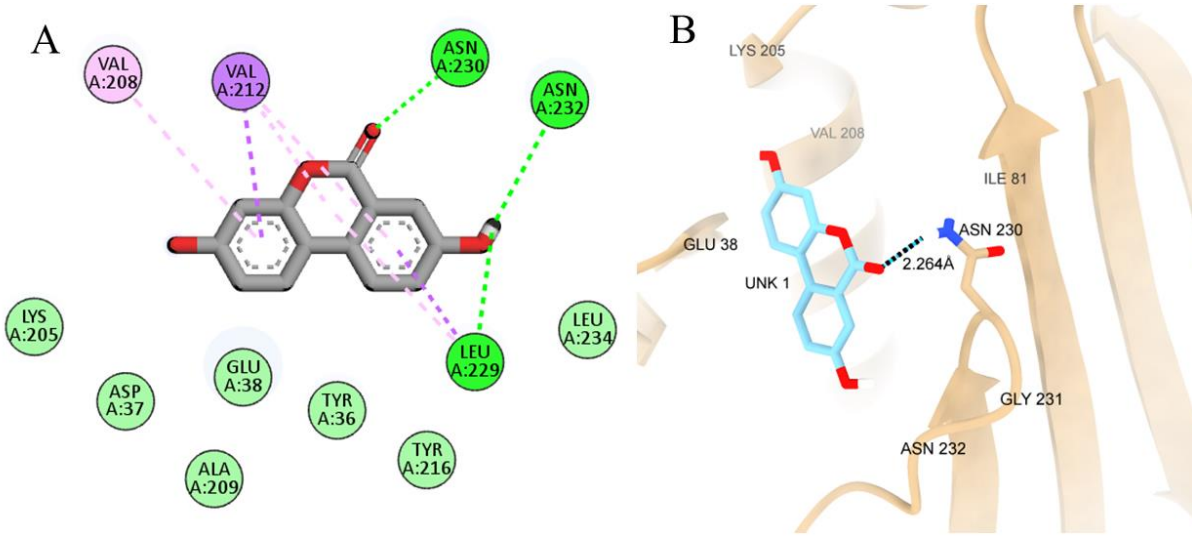

Figure 6: Interaction properties between Urolithin A and Human Topoisomerase IIa ATPase/AMP-PNP (PDB ID: 1ZXM) using Discovery Studio Visualizer (A) and Chimera (B)

(v) Human cytochrome P450 CYP2C9 (protein data bank ID: 1OG5)

The binding profile of Human Cytochrome P450 CYP2C9 (PDB ID: 1OG5) against Urolithin A is shown in Fig. 7. In the Human Cytochrome P450 CYP2C9 (PDB ID: 1OG5) receptor, Urolithin A exhibited a binding affinity of ¯7.9 kcal/mol. The binding energy is attributed to interactions with various amino acids, each contributing through different types of interactions: Van der Waals interactions with VAL[84], ARG[68], GLY[69], ILE[70], PHE[71], GLN[185] and PHE[447]; hydrogen bond with ASN[188], Pi-Pi stacked interactions with PHE[85]; and Pi-Alkyl interactions with LEU[337], PRO[338], ALA[74].

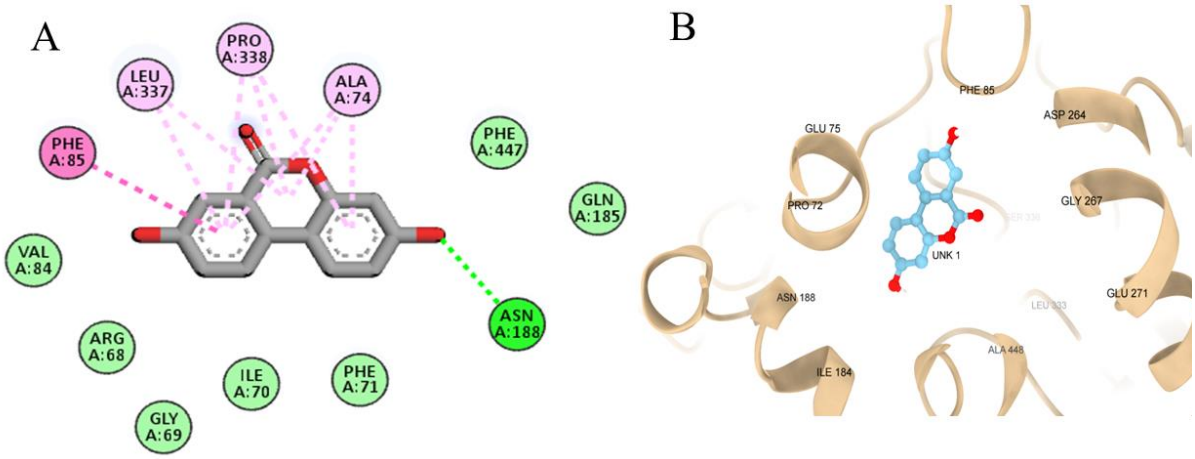

Figure 7: **Interaction properties between Urolithin A and Human Cytochrome P450 CYP2C9 (PDB ID: 1OG5) using Discovery Studio Visualizer (A) and Chimera (B)**

(vi) Epidermal growth factor receptor tyrosine kinase domain with 4-anilinoquinazoline inhibitor erlotinib (protein data bank ID: 1M17)

The binding profile of Epidermal Growth Factor Receptor Tyrosine Kinase Domain with Erlotinib (PDB ID: 1M17) against Urolithin A is shown in Fig. 8. In Epidermal Growth Factor Receptor Tyrosine Kinase Domain with Erlotinib (PDB ID: 1M17) receptor, Urolithin A exhibited a binding affinity of ¯7.7 kcal/mol. The binding energy is attributed to interactions with various amino acids, each contributing different types of interactions: Van der Waals interactions with PHE[28], GLY[101], LEU[23], LEU[97], THR[95] and Pi-Sigma with VAL[31], PI-Alkyl with LYS[50], ALA[48], LEU[149] and hydrogen bond with ASP[160], MET[98].

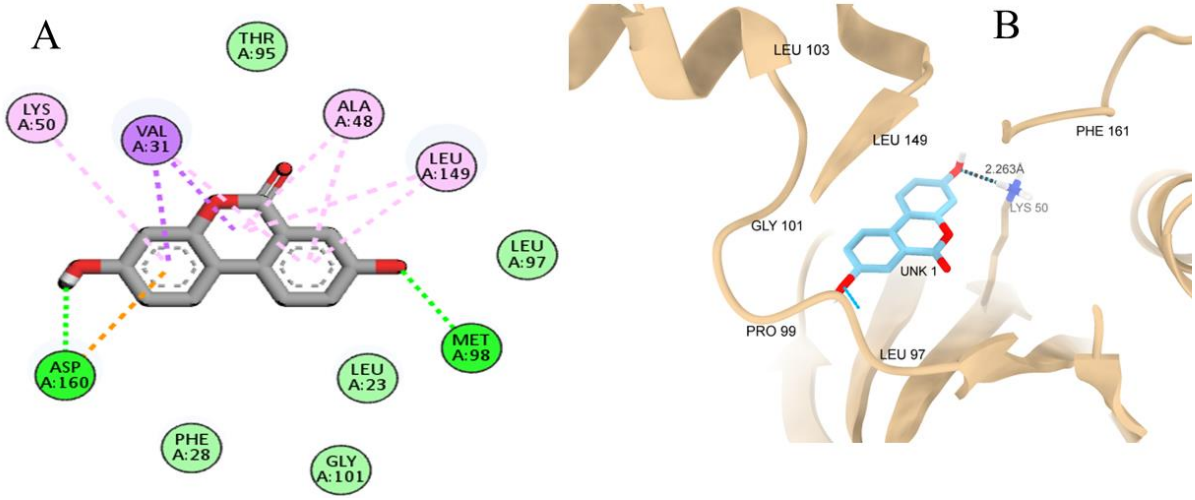

Figure 8: **Interaction properties between Urolithin A and Epidermal Growth Factor Receptor Tyrosine Kinase Domain with Erlotinib (PDB ID: 1M17) using Discovery Studio Visualizer (A) and Chimera (B)**

(vii) Solution structure of Alzheimer's disease amyloid beta-peptide (1-42) (protein data bank ID: 1IYT)

To check on the neurogenesis potential of Urolithin A, the binding profile of amyloid beta-peptide, Human Acetylcholinesterase and Neurotensin Receptor were investigated by docking. The binding profile of the Alzheimer's disease amyloid beta-peptide with PDB ID (1IYT) against Urolithin A is shown in Fig. 9. In Alzheimer's disease, amyloid beta-peptide with PDB ID (1IYT) receptor, Urolithin A, exhibited the finding affinity of ¯5.5 kcal/mol. The binding energy is attributed to interactions with various amino acids, each contributing through different types of interactions: Van der Waals interactions with PHE^{19}, PHE^{20}, H bond with SER^{8}, GLN^{15}, Pi-Sigma with VAL^{12}, and Amide-Pi staked interactions with GLU^{11}.

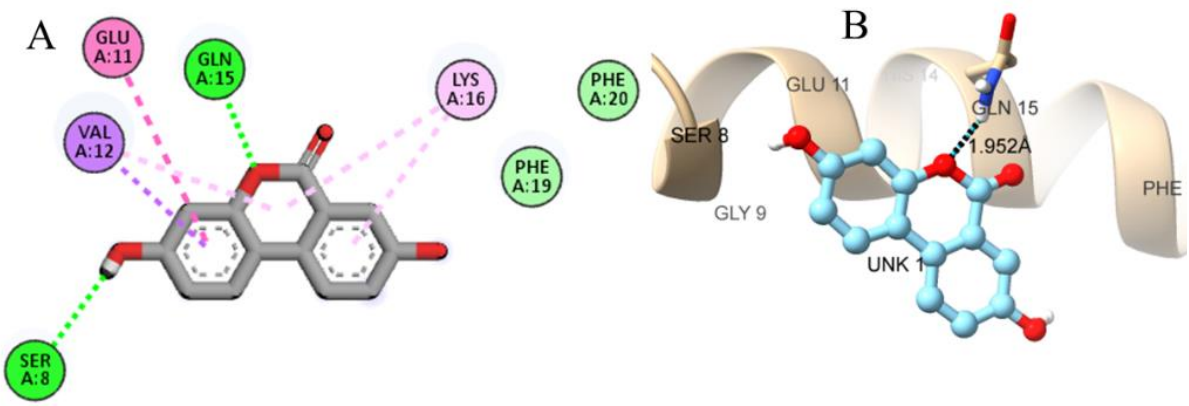

Figure 9: Interaction properties between Urolithin A and Amyloid Beta-Peptide (1-42) (PDB ID: 1IYT) using Discovery Studio Visualizer (A) and Chimera (B)

(viii) Acetylcholinesterase (protein data bank ID: 1B41)

The binding profile of acetylcholinesterase receptor PDB ID (1B41) with Urolithin A is shown in Fig. 10. In the acetylcholinesterase receptor, Urolithin A exhibited a binding affinity of ¯8.8 kcal/mol. The binding energy is attributed to interactions with various amino acids, each contributing through different types of interactions: Van der Waals interactions with VAL^{69}, ASP^{70}, TYR^{120}, TYR^{327}, HIS^{437}, GLY^{438}, SER^{199}, GLU^{198}, ILE^{441}, GLY^{116}, GLY^{117}, GLY^{122}, LEU^{126}, SER^{121}, hydrogen bond with ASN^{83} and Pi-interaction with TRP^{82}.

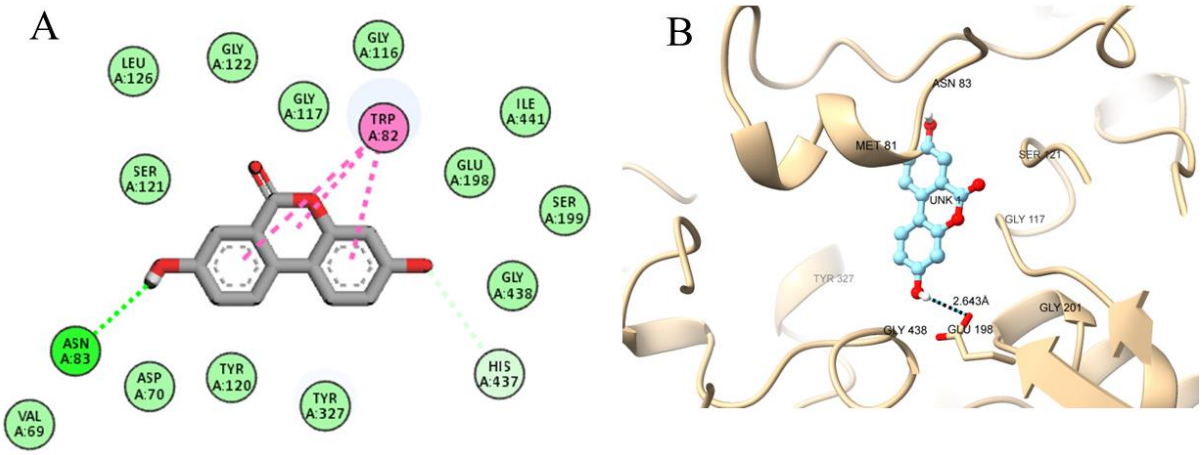

Figure 10: Interaction profile of Urolithin A with Human Acetylcholinesterase (PDB ID: 1B41) active site. Structures visualized with (A) Discovery studio and (B) Chimera

(ix) Neurotensin receptor (protein data bank ID: 1GQR)

In neurotensin Receptor (PDB ID: 1GQR), the binding energy with Urolithin A is ¯9.9 kcal/mol. Notably, various interactions with their contributing residues are shown in Fig. 11. These interactions include Van der Waals forces mediated by TYR^{331}, ASP^{69}, GLY^{120}, GLY^{114}, TYR^{113}, TYR^{127}, ILE^{441}, GLY^{438}, HIS^{437} and Pi-interaction facilitated by PHE^{327} and TRP^{81}.

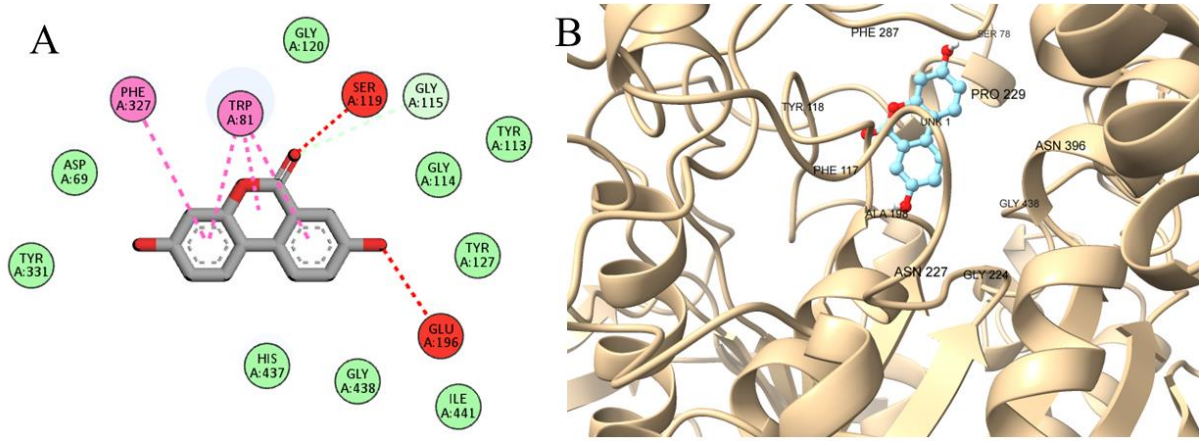

Figure 11: Interaction properties between Urolithin A and Neurotensin Receptor (PDB ID: 1GQR) using Discovery Studio Visualizer (A) and Chimera (B)

(x) Human dipeptidyl peptidase-4 (protein data bank ID: 4EY7)

Human dipeptidyl peptidase-4 (PDB ID 4EY7) exhibits a binding energy of ¯9.7 kcal/mol with Urolithin A. The molecular interactions with contributing residues are shown in Fig. 12. These interactions include Van der Waals forces facilitated by $ALA^{198,}$ SER^{197}, GLY^{438}, TYR^{439}, TRP^{429}, SER^{78}, ASP^{69} and GLY^{114}, Pi-stacking interactions with HIS^{437}, TRP^{81} and PHE^{327} residues, and hydrogen bonding with GLU^{196}, GLY^{115} and TYR^{331}.

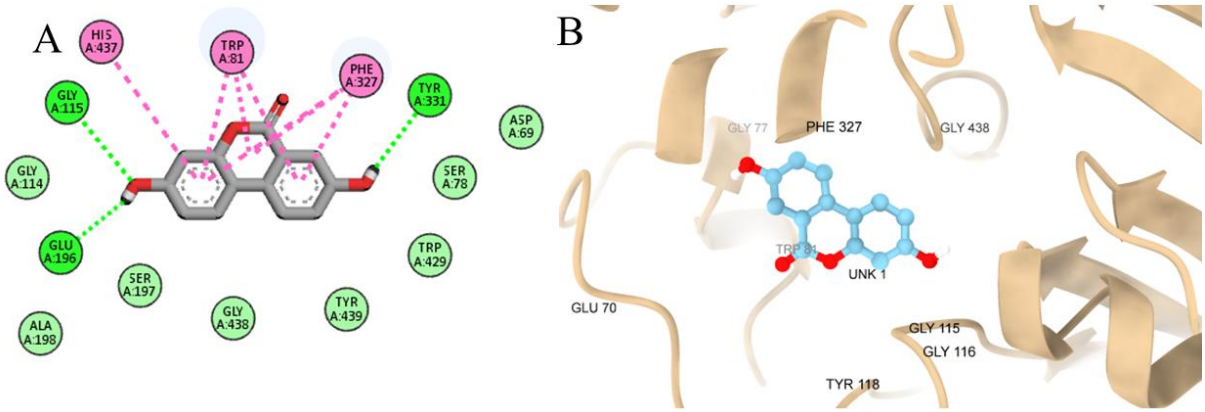

Figure 12: Interaction properties between Urolithin A and Human dipeptidyl peptidase-4 (PDB ID 4EY7 using Discovery Studio Visualizer (A) and Chimera (B)

Table 1: Summary of Urolithin A's binding energy, number and types of molecular interactions, and key interacting residues across protein targets involved in inflammation, oxidative stress, and neurodegeneration

No	Target Protein (PDB ID)	Binding Energy (kcal/mol)	Hydrogen Bonds	π-Interactions (π–π / π–sigma / π–alkyl)	van der Waals Interactions	Key Interacting Residues
1.	p38 MAP kinase in complex with RL87 (4DLI)	⁻10.1	3	2 (π–π, π–sigma)	6	SER^{293}, GLU^{192}, ALA^{255}, SER^{252}, LYS^{249}, ASP^{294}, TRP^{197}, ASN^{196}, ASP^{292}, LEU^{195}, $GLU^{198.}$
2.	Neurotensin Receptor (PDB ID: 1GQR)	⁻9.9	2	2 (π–π)	9	TYR^{331}, ASP^{69}, GLY^{120}, GLY^{114}, TYR^{113}, TYR^{127}, ILE^{441}, GLY^{438}, HIS^{437}, PHE^{327}, $TRP^{81.}$
3.	Human Dipeptidyl Peptidase-4 (PDB ID: 4EY7)	⁻9.7	3	3 (π–π)	8	$ALA^{198,}$ SER^{197}, GLY^{438}, TYR^{439}, TRP^{429}, SER^{78}, ASP^{69}, GLY^{114}, HIS^{437}, TRP^{81}, GLU^{196}, $GLY^{115,}$ PHE^{327}, TYR^{331}.
4.	Acetyl cholinesterase (PDB ID: 1B41)	⁻8.8	1	1 (π–π)	14	VAL^{69}, ASP^{70}, TYR^{120}, TYR^{327}, HIS^{437},

No	Target Protein (PDB ID)	Binding Energy (kcal/mol)	Hydrogen Bonds	π-Interactions (π–π / π–sigma / π–alkyl)	van der Waals Interactions	Key Interacting Residues
						GLY^{438}, SER^{199}, GLU^{198}, ILE^{441}, GLY^{116}, GLY^{117}, GLY^{122}, LEU^{126}, SER^{121}, ASN^{83}, TRP^{82}.
5.	Vioxx Bound to Human COX-2 (PDB ID: 5KIR)	¯8.6	1	2 (π–π)	9	LEU^{391}, PHE^{200}, LEU^{390}, GLN^{203}, TRP^{206}, THR^{206}, PHE^{210}, ASN^{382}, HIS^{386}, ALA^{199}, HIS^{388}, ALA^{202}.
6.	Human Cytochrome P450 CYP2C9 (PDB ID: 1OG5)	¯7.9	1	1 (π–π), 3 (π- Alkyl)	7	VAL^{84}, ARG^{68}, GLY^{69}, ILE^{70}, PHE^{71}, GLN^{185}, PHE^{447}, ASN^{188}, PHE^{85}, LEU^{337}, PRO^{338}, ALA^{74}.
7.	Epidermal Growth Factor Receptor Tyrosine Kinase Domain with 4-anilinoquinazoline inhibitor Erlotinib (PDB ID: 1M17)	¯7.7	2	3 (π–alkyl), 1(π–sigma)	5	PHE^{28}, GLY^{101}, LEU^{23}, LEU^{97}, THR^{95}, VAL^{31}, LYS^{50}, ALA^{48}, LEU^{49},

No	Target Protein (PDB ID)	Binding Energy (kcal/mol)	Hydrogen Bonds	π-Interactions (π–π / π–sigma / π–alkyl)	van der Waals Interactions	Key Interacting Residues
						ASP^{160}, MET^{98}.
8.	Human Topoisomerase IIα ATPase/AMP-PNP (PDB ID: 1ZXM)	¯7.4	3	1 (π–alkyl, π–sigma)	7	LYS^{205}, ASP^{37}, ALA^{209}, GLU^{38}, TYR^{216}, TYR^{36}, LEU^{234}, VAL^{212}, VAL^{205}, LEU^{229}, ASN^{232}, $ASN^{23.}$
9.	Kinase P38/SB203580 complex (PDB ID: 1A9U)	¯6.8	0	3(π–π) 2(π–alkyl)	6	LEU^{74}, LEU^{171}, ILE^{84}, ASP^{168}, TYR^{35}, PHE^{169}, GLU^{71}, LYS^{53}, ARG^{173}, LEU^{75}, ALA^{172}.
10.	Solution structure of Alzheimer's disease Amyloid Beta-Peptide (1-42) (PDB ID: 1IYT)	¯5.5	2	1 (π–π Amide), 1 (π–sigma)	2	PHE^{19}, PHE^{20}, SER^{8}, GLN^{15}, VAL^{12}, GLU^{11}.

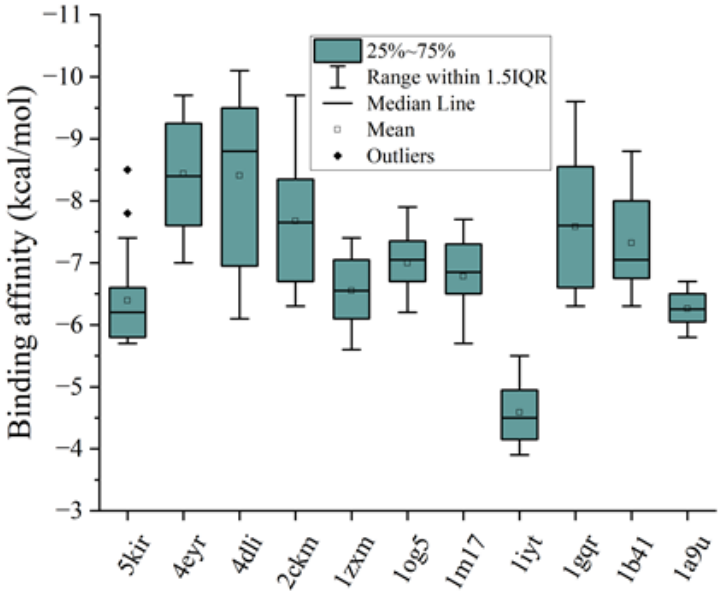

Figure 13: Distribution of Urolithin A binding affinities (kcal/mol) across selected receptors

The midline in each box represents the median, while the small circle denotes the mean binding affinity. The box edges indicate the interquartile range (IQR), and the whiskers extend to 1.5 × IQR. Outliers beyond the whiskers are represented by individual dots. This plot provides a comparative view of docking score distributions across targets.

4.1.2 Conformational stability of Urolithin A with the best candidate receptor

Based on the molecular docking results, several target receptors exhibited promising binding affinities with Urolithin A. Among them, both 4DLI and 4EYR demonstrated similar mean docking scores, as illustrated in the boxplot (Fig. 13). However, 4DLI was selected for molecular dynamics (MD) simulation this decision was guided by statistical and structural considerations. 4DLI exhibited the lowest binding energy (¯10.1 kcal/mol), a narrow interquartile range in docking pose distribution (Fig. 13), which indicated greater consistency and reliability across multiple docking poses. Although the distribution for 4DLI was slightly negatively skewed, suggesting a tail of more favourable binding energies, this was interpreted as an advantage, highlighting the presence of high-affinity interactions within the docking ensemble. Additionally, a qualitative analysis of binding interactions using Discovery Studio revealed that Urolithin A formed stronger and more numerous stabilising interactions, such as hydrogen bonds and π–π stacking, within the active site of 4DLI compared to other receptor targets. This combination of statistical and visual criteria informed the decision to advance 4DLI for further structural and dynamic stability assessment through MD simulations.

(i) Root mean square deviation

To assess the stability and conformation changes of Human p38 MAP kinase (4DLI) upon Urolithin A binding, the Root Mean Square Deviation (RMSD) of the apo protein (unbound) and complex protein (Urolithin A-bound) structure were calculated over a 100 ns simulation timeframe. The results are presented in Fig. 14. In Fig. 14 (A), the RMSD profiles reveal that the apo protein exhibited consistent stability of 0.2 nm throughout the 100 ns timeframe, with minor fluctuations occurring within the normal range of approximately 0.05 nm. For the Human p38 MAP kinase and Urolithin A complex, a diverse RMSD range was observed. The average distance for the first 10 ns was 0.5 nm, then dropped to 0.4 nm for the second 10 ns. The distance decreased to 0.3 nm, where it converged with that of the apo protein at 20-25 ns. For the next 25 ns, the distance rose to 0.5 nm, while at 50-70 ns, a gradual increase of distance from 0.5 to 0.7 nm was observed. Lastly, at 80-100 ns, 0.7 was maintained. Figure 14 (B) shows the probability distribution of RMSD (P (rmsd)) in the apo and complex protein. The P (rmsd) highlights the conformational preference of the apo and complex protein at the 100 ns timeframe. In the apo protein, the preference for one conformation is observed at 0.4 nm, while the complex protein has two conformations at 0.2 and 0.6 nm. Thus, the RMSD suggests that the interaction between human p38 MAP kinase and Urolithin A induces conformational changes while the overall structure of the apo protein remains unchanged. In this study, RMSD was applied to monitor the stability of Urolithin A complexes with p38 MAP kinase. A plateaued RMSD curve indicated successful equilibration and stable interactions.

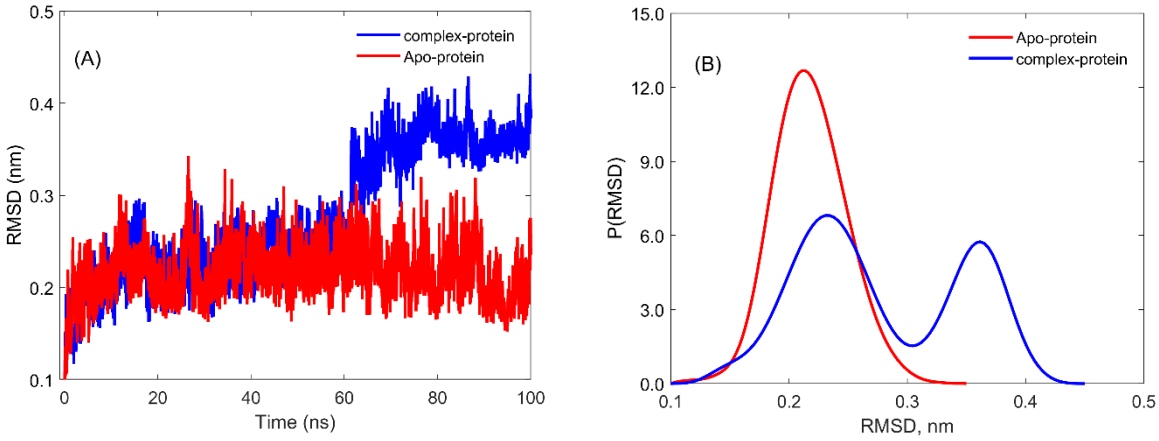

Figure 14: Time-dependent RMSD (A) and (B) probability distribution of RMSD for the Human p38 MAP kinase and Urolithin A, apo and complex during 100-ns MD simulation

(ii) The root mean squared fluctuations

An RMSF analysis was conducted to analyse residue flexibility following the addition of Urolithin A, and the results are shown in Fig. 15. In the apoprotein, most fluctuation intensities remained below 0.3 nm, except for specific residues: The TYR^{29} with 0.5 nm, ARG^{51} with 0.3 nm, LYS^{113} with 0.3 nm, GLU^{152} with 0.3 nm, TYR^{180} with 0.3 nm, GLN^{244} with 0.3 nm, PHE^{307} with 0.3 nm, LEU^{333} with 0.3 nm, ASP^{334} with 0.5 nm. In the complex protein, most residues that exhibited greater than 0.3 nm fluctuation in the apoprotein showed a reduction in fluctuation values. These residues include TYR^{29} with 0.23 nm, ARG^{51} with 0.18 nm, LYS^{113} with 0.18 nm, GLU^{152} with 0.14 nm, TYR^{180} with 0.10 nm, GLN^{244} with 0.25 nm, PHE^{307} with 0.15 nm. However, contrary to this trend, residues LEU^{333} with 1.15 nm and ASP^{334} with 1.37 nm exhibited increased fluctuations compared to the apoprotein structure. Therefore, the reduced fluctuation observed in complex structure signifies increased protein stability influenced by the presence of Urolithin A.

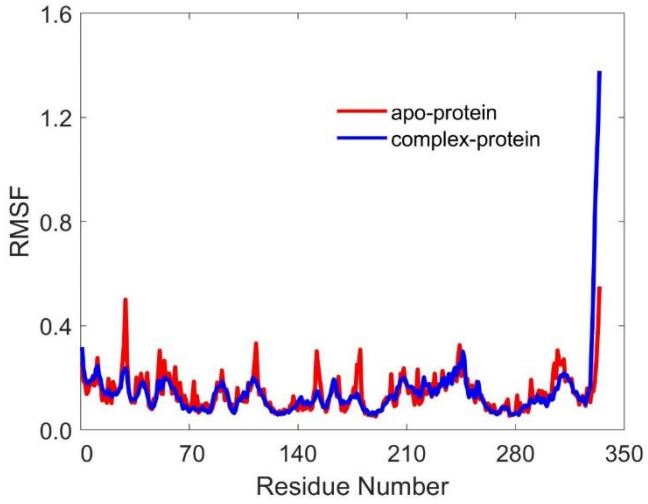

Figure 15: The RMSF of Human p38 MAP kinase and Urolithin A complex during 100-ns MD simulation

(iii) Radius of gyration

To assess the effect of Urolithin A on compactness of the Human p38 MAP kinase structure, the radius of gyration was conducted, and the results are shown in Fig. 16. In Fig. 16 (A), the Rg value for apoprotein was 2.3 nm at 0-10 ns. For the next 10 ns, the value dropped to 2.2 nm and then increased to 2.3, remaining unchanged to 100 ns. The Human p38 MAP kinase and Urolithin A complex show varied values of radius of gyration. For the first 20 ns, a gradual drop in Rg value is observed from 2.2 – 2.1 nm. A gradual rise of Rg is observed from 20-70 ns from 2.1 to 2.3 nm, a value where the complex Rg converges with the apo structure. From

the observation above, the complex formed by Human p38 MAP kinase and Urolithin A exhibits a smaller gyration radius than that of the apo structure. This observation is a key indicator of the structural stability and compactness of the three-dimensional protein structure, considering that the smaller the Rg value, the more compact the structure. Figure 16 (B) shows the probability distribution of Rg (P(rg)) in apo and complex protein. The P(rg) highlights the conformation preference of apo and complex protein at a 100 ns time frame. In the apoprotein, the preference of one conformation is observed at 2.20 nm, while complex protein had conformation at 2.25 nm. Therefore, the smaller value of Rg suggests that the interaction between Human p38 MAP kinase and Urolithin A results in compact conformation, while the larger Rg value of the apoprotein results in an extended conformation.

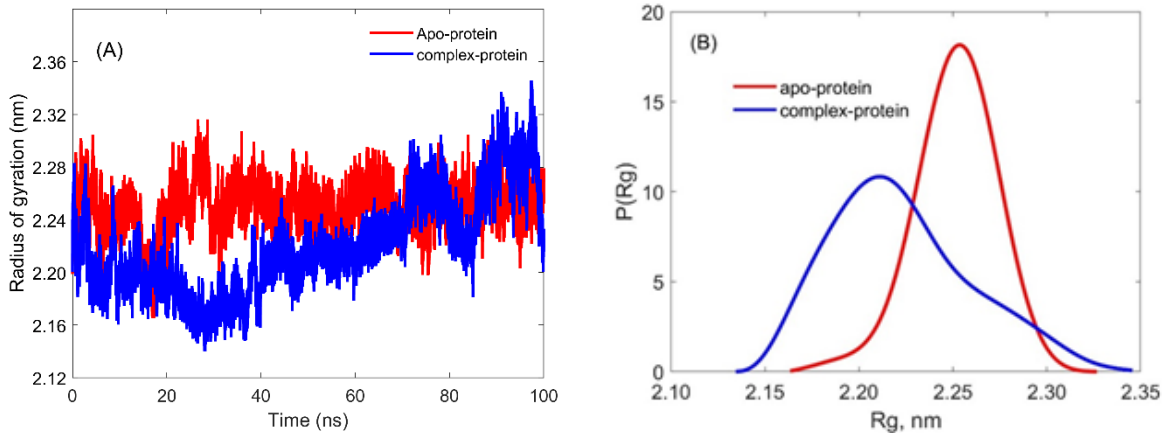

Figure 16: Time-dependent Rg (A) and (B) probability distribution of Rg for the Human p38 MAP kinase and Urolithin A, apo and complex during 100-ns MD simulation

(iv) Number of hydrogen bonds

An analysis of hydrogen bond count on the trajectory of Urolithin A with the human p38 MAP kinase was conducted to confirm the key role of hydrogen bond interactions in optimal binding. The results are shown in Fig. 17. The analysis revealed the presence of an average of three hydrogen bond interactions for the first 40 ns timeframe, followed by a drop to one hydrogen bond over 40-60 ns, and finally, a rise to an average of three hydrogen bonds to 100 ns. These findings highlight the dynamic nature of hydrogen bond interactions and their critical role in the stability and binding affinity of Urolithin A with the human p38 MAP kinase.

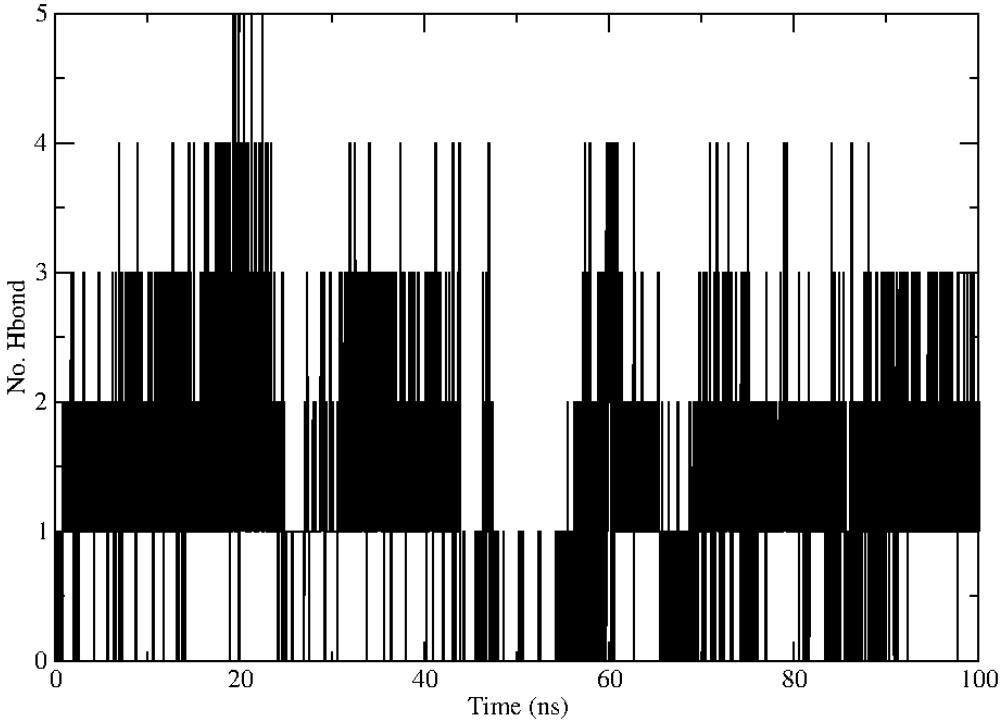

Figure 17: The number of hydrogen bonds (Hydrogen bond) Human p38 MAP kinase and Urolithin A during 100-ns MD simulation

4.1.3 Solvent Accessible Surface Area

To compute the solvent accessibility surface area (SASA) on Urolithin A with the human p38 MAP kinase complex, SASA measures the surface area of the protein accessible to solvent. Indicates protein compactness and exposure of residues to the solvent. Apo-protein shows lower SASA compared to the complex. The increased SASA in the Urolithin A-bound complex suggests potential conformational expansion or surface rearrangement upon ligand binding. This may reflect a reorganisation of surface residues to accommodate the ligand, possibly exposing some previously buried regions. SASA results shown in Fig.18. The analysis of SASA provides insights into the exposure of the protein surface to solvent molecules in both the apo (unbound) and Urolithin A-bound (complex) states. Figure 18 (A) depicts the SASA values, which are which are 175 nm^2 and 178 nm^2 for complex-protein and apo-protein, respectively. Interestingly, the SASA of the complex shows a slight decrease compared to the apo protein. This observation suggests a minimal change in the overall solvent exposure upon Urolithin A's binding to the active site. The complex exhibits slightly more consistent SASA values after ~20 ns, indicating a stable binding conformation may have formed.

Figure 18 (B) illustrates the probability distribution of the Accessible Surface Area of free Human p38 MAP kinase protein compared to that bound to Urolithin A. The graph indicates that the apo-protein tends to favour a conformation with increased surface area, exposing more

residues to the solvent environment. In contrast, the complex protein tends to adopt a conformation with a reduced surface area, with residues buried in hydrophobic parts and less interaction with the solvent environment. This observation of the trend in the probability distribution of apo and complex protein values aligns with the observation from Fig. 18 (B), which depicts the SASA values. Generally, increased stability in a protein-ligand complex is associated with decreased solvent-accessible surface area (SASA). This is because a more stable complex typically involves tighter binding and more compact conformation, reducing the surface area exposed to the solvent. Therefore, lower SASA values usually indicate a more stable and tightly bound complex.

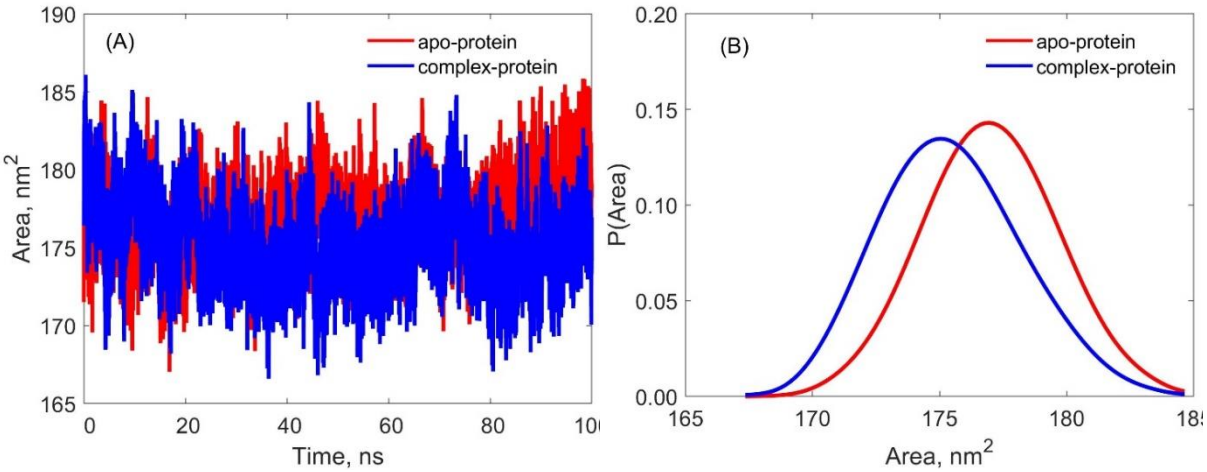

Figure 18: Time-dependent SASA (A) and (B) probability distribution of SASA for the Human p38 MAP kinase and Urolithin A, apo and complex during 100-ns MD simulation

4.2 Discussion

The docking simulations provided valuable insights into the interactions between Urolithin A and various target proteins. Binding energies were calculated to assess the affinity between Urolithin A and each receptor. Generally, binding energies below ¯6.0 kcal/mol are considered indicative of good affinity for a therapeutic product molecule (Nath *et al.*, 2021). In this study, all targeted proteins except Alzheimer's disease Amyloid Beta-Peptide, displayed favourable binding energies ranging from ¯5.5 to ¯10.1 kcal/mol. Notably, human p38 MAP kinase (PDB ID: 4DLI) in complex with Urolithin A exhibited the strongest interaction with Urolithin A, reflected by a binding energy of ¯10.1 kcal/mol. This value surpasses the ¯7.8 kcal/mol binding energy reported for a carothrixin B derivative complexed with human p38 MAP kinase using Autodock vina (Long *et al.*, 2021). The analysis of the interaction profile revealed that Urolithin A forms both polar and non-polar interactions with human p38 MAP kinase. Notably, van der Waals interaction was observed between Urolithin A and residue SER^{293}. This finding

differs from the previous report by Long *et al.* (2021), where SER^{293} was identified as a key hydrogen bond residue stabilising the p38 MAP kinase complex with a leukaemia-derived inhibitor.

The P38α Mitogen-activated protein kinases (MAPK) residues interacting with Urolithin A as TYR^{35}, LYS^{53}, GLU^{71} and ASP168. These residues are important in molecular recognition, especially for anti-inflammation effects. In line with that, TYR^{35} and LYS^{53} residues were key residues in MAPK receptor interaction with successful inhibitor candidates obtained after a virtual screening of 3622 candidates with active and inactive properties (Yang *et al.*, 2022). Residue LYS^{53} interacted with low binding energy synthesized N-[3-(substituted-4H-1,2,4-triazol-4-yl)]-benzo[d]thiazol-2-amines through molecular docking by Tariq *et al.* (2018). Similarly, in Gangwal *et al.* (2014), LYS^{53}, GLU^{71} and ASP168 residues were key in inhibiting P38α Mitogen-activated protein kinases through virtual screening of inhibitors filtered from databases. These findings highlight the importance of TYR^{35}, LYS^{53}, GLU^{71} and ASP^{168} amino acid residues in binding and inhibiting P38α MAPK, underscoring their potential as targets for developing anti-inflammatory therapeutic products. The consistency of key residue involvement across different studies reinforces the reliability of these targets in therapeutic product design.

Cyclooxygenase-2 (COX-2) is an essential enzyme accountable for the change of arachidonic acid into prostaglandins, which are known to mediate inflammatory processes. As such, COX-2 is a deep-rooted target for emerging anti-inflammatory medications (Jain *et al.*, 2023). In this study, Urolithin A demonstrated a binding energy of ¯8.6 kcal/mol, suggesting promising anti-inflammatory potential. This value falls within the range observed for potent (AGP) (*Andrographis paniculata*) derivatives, which are effective anti-inflammatory agents (Harinie, 2022). Notably, Urolithin A exhibited a superior binding affinity compared to established COX-2 inhibitors, such as aspirin and recofixib pharmaceuticals, whose binding energies were reported to be ¯5.61 and ¯8.17 kcal/mol, respectively (Jiao *et al.*, 2019; Lee *et al.*, 2011; Yuan *et al.*, 2016). The analysis of the binding site revealed an interaction between Urolithin A and residue TRP^{387}, a key amino acid known to be critical for COX-2 function. This observation mirrors the interaction pattern observed between COX-2 and the recofixib.

Topoisomerases are essential nuclear enzymes responsible for creating temporary breaks in DNA strands (Zagnoli-Vieira & Caldecott, 2020). These breaks are crucial for various cellular processes, such as DNA replication, transcription and repair. However, the oxidation process

can generate reactive oxygen species (ROS) that damage DNA, including the DNA breaks induced by topoisomerases (Shi & Dansen, 2020). Consequently, this oxidative stress can exacerbate DNA damage and hinder the normal functioning of topoisomerases. The CYP2C9 is a vital enzyme within the cytochrome P450 family, playing a significant role in the oxidative metabolism of both foreign (xenobiotic) and native (endogenous) compounds (Singh *et al.*, 2023). It accounts for approximately 18% of the cytochrome P450 proteins in liver microsomes. The CYP2C9, an enzyme crucially involved in metabolism and various physiological processes, is primarily expressed in the liver but is also found in the duodenum and small intestine (Zhao *et al.*, 2021). Docking simulations predicted a binding energy of ¯7.9 kcal/mol between CYP2C9-1OG5 and Urolithin A. This value is higher than the ¯7.4 kcal/mol binding energy reported for 1-hydroxy-2,3,5-trimethoxy-xanthone (HM-1), an active constituent of *Halenia elliptica*, when docked with CYP2C9-1OG5 (Feng *et al.*, 2012). These results suggest that Urolithin A may have a stronger inhibitory effect on CYP2C9-1OG5 compared to HM-1 inhibitors. Interestingly, the key interactions between Urolithin A and CYP2C9-1OG5 involve hydrogen bonds, mirroring the interactions observed for HM-1 (Feng *et al.*, 2012). These observations align with the reported inhibitory patterns of successful CYP2C9 inhibitors, suggesting a potentially similar inhibitory mechanism for Urolithin A.

Urolithin A's potential as an antioxidant was investigated through its interaction with Epidermal Growth Factor Receptor (EGFR) tyrosine kinase. Docking simulations revealed a binding energy of ¯7.7 kcal/mol, suggesting a potential role in EGFR inhibition. This value falls within the range reported in two dihydroquinoline-4-carboxylic derivatives (¯7.4 and ¯7.8 kcal/mol) using X-ray crystallographic and spectroscopic techniques (Hayani *et al.*, 2021). The antioxidant properties of quinolines are attributed to their capacity to donate hydrogen atoms or electrons to reactive oxygen species (ROS), thereby neutralising their harmful effects (Uddin *et al.*, 2021). The presence of nitrogen atoms within the quinoline ring further enhances this electron-donating ability, leading to more efficient free radical scavenging and protection of biomolecules from oxidative damage (Zahrani *et al.*, 2020). Moreover, the inherent aromaticity of quinoline contributes to the stability of radicals formed during these processes. Similar to quinolines, Urolithin A possesses antioxidant properties due to its ability to donate electrons or hydrogen atoms to reactive oxygen species (ROS) (Kallio *et al.*, 2013). The presence of oxygen functional groups in the Urolithin structure facilitates this electron donation, thereby enhancing its free radical scavenging activity and protecting biomolecules from oxidative stress (Ito, 2011; Ito *et al.*, 2008). Furthermore, the inherent structural features of Urolithin molecules

contribute to the stability of radicals generated during ant oxidation processes, thereby bolstering their overall antioxidant potential.

Amyloid-β is a protein central to Alzheimer's disease, a prevalent neurodegenerative disorder characterised by its accumulation in the brain (Hampel *et al.*, 2021). The Aβ aggregation disrupts neuronal function and contributes to cognitive decline (Ju *et al.*, 2022). Targeting Aβ is a promising strategy for treating Alzheimer's disease (Zhang *et al.*, 2023). Although Urolithin A demonstrated promising binding affinities with several targets, its interaction with Amyloid Beta-Peptide (PDB ID: 1IYT) yielded a comparatively moderate binding energy of ¯5.5 kcal/mol. This lower affinity may be attributed to several structural and methodological factors. Structural analysis using Discovery Studio revealed that Urolithin A failed to form strong π–π stacking interactions with key aromatic residues such as PHE^{20}, which are crucial in the stabilisation of Aβ aggregates (Rubavathy & Prakash, 2025).

The ligand's partially polar structure, characterized by hydroxyl groups, appeared to be suboptimal for the narrow and predominantly hydrophobic binding cleft of 1IYT. Furthermore, the lack of deep hydrogen bonding and the absence of salt-bridge formation within the binding site may have contributed to weaker receptor-ligand interactions. It is also important to consider limitations in the docking protocol, such as receptor rigidity and exclusion of solvent dynamics, which may not fully capture the flexible nature of the amyloid peptide or the potential of Urolithin A under physiological conditions.

These observations highlight that while Urolithin A may hold therapeutic promise for targets involved in oxidative stress and inflammation, its neuroprotective efficacy against Aβ aggregation may be limited due to suboptimal binding characteristics. While this value suggests moderate affinity, it is lower compared to the ¯9.087 kcal/mol binding energy reported for Pregnenolone derivative (Tahir *et al.*, 2024). Interestingly, Urolithin A interacts with Amyloid-β through both hydrophobic and hydrophilic interactions involving the key PHE^{20} residue. This finding aligns with observations for Pregnenolone derivatives, where PHE^{20} was identified as a key residue for hydrophobic interactions that hinder Aβ β-sheet formation (Pasieka *et al.*, 2021; Umar *et al.*, 2019).

Root Mean Squared Deviation (RMSD) analysis was employed to assess the impact of Urolithin A's binding on the structural fluctuations of human p38 MAP kinase. The RMSD profile revealed a gradual increase in RMSD from 0.2 nm at the beginning of the simulation

(50 ns) to approximately 0.4 nm at the end (100 ns). This observation suggests that Urolithin A binding induces a time-dependent conformational shift in the protein structure. However, it is important to note that the RMSD values remained within a relatively narrow range (0.2-0.4 nm, i.e., not more than 0.5 nm for 100 ns) throughout the simulation, indicating that the overall structural integrity of the protein was preserved. Notably, this range aligns well with the findings reported by Chen *et al.* (2021) for the RMSD of the p38 MAP kinase (0.12-0.49 nm) targeted by three structurally similar inhibitors.

Root Mean Squared Fluctuation was conducted to assess the impact of Urolithin A on the flexibility of MAP 38 kinase. The RMSF profile revealed changes in residue flexibility upon Urolithin A binding. Compared to the apo protein, the complex structure exhibited generally lower RMSF values than the apo protein, indicating a more rigid structure. This observation aligns with previous findings by Chen *et al.* (2021), who demonstrated that inhibitor binding to a similar MAPK p38 receptor resulted in a structure with reduced RMSF compared to the apo form. In their study, most residues displayed an RMSF around 0.2 nm, suggesting decreased flexibility and enhanced stability. The lower RMSF values observed in the present study further support the notion that Urolithin A binding stabilises human p38 MAP kinase, potentially contributing to its anti-inflammatory properties.

The radius of gyration (Rg) is a metric that reflects the protein's overall compactness and conformational stability. A lower Rg value typically indicates a more compact and stable structure. In the context of ligand binding, a decrease in Rg suggests a conformational shift towards a tighter and more compact protein-ligand complex. The observed reduction in Rg for the human p38 MAP kinase-Urolithin A. The observed decrease in Rg for the human p38 MAP kinase-Urolithin A aligns with this notion, implying that Urolithin A binding induces a conformation that is more compact than the apo form. This finding is supported by previous work by Aasiya *et al.* (2023), who reported a similar Rg value of approximately 2.25 nm for 1,2,4-triazole 4,3-a pyridine analogues that successfully inhibited inflammation. Furthermore, the trend observed in the Rg of the complex compared to the apo structure is consistent with the SASA data, suggesting a minimal change in overall solvent exposure upon Urolithin A binding.

CHAPTER FIVE

CONCLUSION AND RECOMMENDATIONS

5.1 Conclusion

This study's findings shed light on the promising therapeutic implications of Urolithin A in addressing a wide range of inflammatory, oxidative, and neurodegenerative conditions through its interactions with specific target receptors. Through docking analysis, Urolithin A has demonstrated diverse binding affinities across different targets, with particularly strong interactions observed with the 4DLI receptor, showcasing its potential efficacy (binding affinity of -10.1 kcal/mol). Visualising the binding interactions has provided valuable insights into the molecular mechanisms underlying Urolithin A's therapeutic effects and efficacy.

In the context of inflammatory targets, Urolithin A has demonstrated significant binding affinities with receptors such as 1A9U and 5KIR, indicating its potential to mitigate inflammatory responses. Similarly, Urolithin A's promising interactions observed with receptors like 1ZXM, 1OG5, and 1M17 concerning oxidant targets suggest its antioxidant properties. Moreover, in neurodegenerative research, Urolithin A has displayed favourable binding affinities with targets associated with Alzheimer's disease and acetylcholinesterase, indicating its potential to mitigate neurodegenerative processes.

Subsequent molecular dynamics simulations have highlighted the stability of the Human p38 MAP kinase and Urolithin A complex, with minor local conformational changes induced by Urolithin A. Analysis of RMSD, RMSF and radius of gyration has indicated consistent stability and minimal fluctuations within the protein-ligand complex, thereby supporting the integrity of the interaction. Furthermore, analysis of hydrogen bonds and hydrophobic interactions has underscored the specificity and stability of the ligand-protein interaction, elucidating the dynamic nature of the binding process. The analysis of SASA has provided insights into alterations in residue accessibility induced by the protein-ligand interaction, thereby enhancing our understanding of the molecular mechanisms involved.

Overall, these findings highlight the potential therapeutic value of Urolithin A in combating inflammatory, oxidative and neurodegenerative conditions through its interactions with specific target receptors. Further research and clinical studies are warranted to validate these findings and elucidate the precise mechanisms underlying Urolithin A's therapeutic effects, paving the way for developing novel treatments for these debilitating conditions.

5.2 Recommendations

Based on the research findings, the following recommendations are proposed:

(i) *Expand Molecular Dynamics Simulations*: Future studies should extend MD simulations to include additional high-affinity targets such as COX-2 and Acetylcholinesterase to comprehensively validate Urolithin A's multi-target potential and assess the dynamic stability of these complexes.

(ii) *Further experimental validation*: The computational simulations have shown promising results regarding the therapeutic potential of Urolithin A in treating inflammatory, oxidative, and neurodegenerative conditions. However, to validate these findings and ascertain Urolithin A's efficacy, further experimental validation through in vitro and in vivo studies is crucial. These studies will not only confirm the predicted binding interactions but also provide insights into the biological mechanisms underlying Urolithin A's effects.

(iii) *Exploration of combination therapies*: Considering the diverse range of targets identified in this study, exploring combination therapies involving Urolithin A with other therapeutic agents could enhance efficacy and potentially mitigate adverse effects. Investigating synergistic interactions between Urolithin A and existing treatments for inflammatory and neurodegenerative diseases may lead to novel therapeutic strategies tailored to specific conditions.

(iv) *Optimisation of Urolithin A derivatives*: Structural modifications and optimisation of Urolithin A derivatives based on the observed binding interactions could enhance its pharmacokinetic properties, bioavailability, and target specificity. Rational nutraceuticals design approaches, informed by computational modelling and structure-activity relationship studies, can facilitate the development of more potent and selective Urolithin A analogues with improved therapeutic profiles.

(v) *Perform Experimental Validation*: Experimental methods such as surface plasmon resonance, isothermal titration calorimetry, or cell-based assays should be employed to validate the computational predictions, particularly regarding receptor-ligand stability and functional efficacy.

(vi) *Utilize Multi-target Simulation Models*: Incorporating systems biology or network pharmacology approaches could offer insights into how Urolithin A modulates interconnected signaling pathways, especially for age-related degenerative diseases.

(vii) *Optimize Docking Protocols*: Advanced scoring functions and ensemble docking across multiple protein conformations could enhance the accuracy of docking predictions and help reduce possible biases introduced by rigid receptor structures.

(viii) *Encourage Integration with Gut Microbiota Models:* Since Urolithin A is a microbial-derived metabolite, future research could explore microbiota-host-drug interaction models to capture its bioavailability and systemic effects more holistically.

(ix) Additionally, future work should consider incorporating Free Energy Landscape (FEL) analysis to further understand the conformational transitions and thermodynamic stability of Urolithin A-receptor complexes. This technique provides deeper insight into the energy minima and transition states during molecular dynamics simulations, which can help validate and complement RMSD, Rg, RMSF and SASA analyses.

REFERENCES

Aasiya, C., Mangala, K., Chandrakant, B., Muthal, A., & Kulkarni, R. (2023). Investigation of structure–activity relationship: In silico studies of [1,2,4]-triazolo[4,3-a]pyridine ureas as P38 kinase inhibitors. *Structural Chemistry, 34*(3), 915–929.

Abramowicz, M. A., Miller, J. C., & Stuchlík, Z. (1993). Concept of radius of gyration in general relativity. *Physical Review D, 47*(4), 1440.

Adwas, A. A., Elsayed, A., Azab, A. E., & Quwaydir, F. A. (2019). Oxidative stress and antioxidant mechanisms in human body. *Journal of Applied Biotechnology & Bioengineering, 6*(1), 43–47.

Alara, O. R., Abdurahman, N. H., & Ukaegbu, C. I. (2021). Extraction of phenolic compounds: A review. *Current Research in Food Science, 4*, 200–214.

Allinger, N. L. (2010). *Molecular Structure: Understanding Steric and Electronic Effects from Molecular Mechanics*. John Wiley & Sons.

Alturki, F. A., Omotoso, H. O., Al-Shamma'a, A. A., Farh, H. M., & Alsharabi, K. (2020). Novel manta rays foraging optimization algorithm based optimal control for grid-connected PV energy system. *IEEE Access, 8*, 187276–187290.

Amadei, A., Linssen, A. B., & Berendsen, H. J. (1993). Essential dynamics of proteins. *Proteins: Structure, Function, and Bioinformatics, 17*(4), 412–425.

Arvanitakis, Z., Shah, R. C., & Bennett, D. A. (2019). Diagnosis and management of dementia. *JAMA, 322*(16), 1589–1599.

Atkin, N. D., Raimer, H. M., & Wang, Y. H. (2019). Broken by the cut: A journey into the role of topoisomerase II in DNA fragility. *Genes, 10*(10), 791.

Ausaf-Ali, S., Imtaiyaz-Hassan, M., Islam, A., & Ahmad, F. (2014). A review of methods available to estimate solvent-accessible surface areas of soluble proteins in the folded and unfolded states. *Current Protein & Peptide Science, 15*(5), 456–476.

Bachli, M. B., Sedeño, L., Ochab, J. K., Piguet, O., Kumfor, F., Reyes, P., Torralva, T., Roca, M., Cardona, J. F., & Campo, C. G. (2020). Evaluating the reliability of neurocognitive

biomarkers of neurodegenerative diseases across countries: A machine learning approach. *NeuroImage, 208*, 116456.

Bader, R. F. (1998). A bond path: A universal indicator of bonded interactions. *The Journal of Physical Chemistry A, 102*(37), 7314–7323.

Bai, R., Yao, C., Zhong, Z., Ge, J., Bai, Z., Ye, X., Xie, T., & Xie, Y. (2021). Discovery of natural anti-inflammatory alkaloids: Potential leads for drug discovery for the treatment of inflammation. *European Journal of Medicinal Chemistry, 213*, 113165.

Belubbi, A. V., & Martis, E. A. (2017). *Advanced Techniques in Biomolecular Simulations. In Handbook of Research on Medicinal Chemistry: Innovations and Methodologies* (Vol. 71). https://scholar.google.com/

Berdowska, I., Matusiewicz, M., & Fecka, I. (2021). Punicalagin in cancer prevention via signaling pathways targeting. *Nutrients, 13*(8), 2733.

Bernath, P. F. (2020). *Spectra of Atoms and Molecules*. Oxford University Press. https://scholar.google.com

Bindu, S., Mazumder, S., & Bandyopadhyay, U. (2020). Non-steroidal anti-inflammatory drugs (NSAIDs) and organ damage: A current perspective. *Biochemical Pharmacology, 180*, 114147.

Boggia, R., Turrini, F., Roggeri, A., Olivero, G., Cisani, F., Bonfiglio, T., Summa, M., Grilli, M., Caviglioli, G., & Alfei, S. (2020). Neuroinflammation in aged brain: Impact of the oral administration of ellagic acid microdispersion. *International Journal of Molecular Sciences, 21*(10), 3631.

Bon, V., Brunner, E., Pöppl, A., & Kaskel, S. (2020). Unraveling structure and dynamics in porous frameworks via advanced in situ characterization techniques. *Advanced Functional Materials, 30*(41), 1907847.

Bravo, L. (1998). Polyphenols: Chemistry, dietary sources, metabolism and nutritional significance. *Nutrition Reviews, 56*(11), 317–333.

Broad, J., Preston, S., Wheatley, R. J., & Graham, R. S. (2021). Gaussian process models of potential energy surfaces with boundary optimization. *The Journal of Chemical Physics, 155*(14).

Cao, G., Liu, J., Liu, M., & Liang, W. (2023). Effects of the COVID-19 pandemic on life expectancy at birth at the global, regional and national levels: A joinpoint time-series analysis. *Journal of Global Health, 13*, 04001.

Cásedas, G., Les, F., Choya-Foces, C., Hugo, M., & López, V. (2020). The metabolite urolithin-A ameliorates oxidative stress in neuro-2a cells, becoming a potential neuroprotective agent. *Antioxidants, 9*(2), 177.

Cesari, M., Sumi, Y., Han, Z. A., Perracini, M., Jang, H., Briggs, A., Thiyagarajan, J. A., Sadana, R., & Banerjee, A. (2022). Implementing care for healthy ageing. *BMJ Global Health, 7*(2), e007778.

Chauhan, A., & Chauhan, V. (2020). Beneficial effects of walnuts on cognition and brain health. *Nutrients, 12*(2), 550.

Chen, J., Wang, W., Sun, H., Pang, L., & Bao, H. (2021). Binding mechanism of inhibitors to p38α MAP kinase deciphered by using multiple replica Gaussian accelerated molecular dynamics and binding free energy calculations. *Computers in Biology and Medicine, 134*, 104485.

Chitadze, G., Wehkamp, U., Janssen, O., Brüggemann, M., & Lettau, M. (2021). The serine protease CD26/DPP4 in non-transformed and malignant T cells. *Cancers, 13*(23), 5947.

Cullen, C. M., Aneja, K. K., Beyhan, S., Cho, C. E., Woloszynek, S., Convertino, M., McCoy, S. J., Zhang, Y., Anderson, M. Z., & Alvarez-Ponce, D. (2020). Emerging priorities for microbiome research. *Frontiers in Microbiology, 11*, 491374.

D'Amico, D., Andreux, P. A., Valdés, P., Singh, A., Rinsch, C., & Auwerx, J. (2021). Impact of the natural compound Urolithin A on health, disease and aging. *Trends in Molecular Medicine, 27*(7), 687–699.

D'Amico, D., Fouassier, A., Faitg, J., Hennighausen, N., Brandt, M., Konstantopoulos, D., Rinsch, C., & Singh, A. (2023*). Topical Application of Urolithin a Slows Intrinsic Skin*

Aging and Protects From UVB-Mediated Photodamage: Findings from Randomized Clinical Trials. Medrxiv. *Advance Online Publication.* https://scholar.google.com/

Daly, A. K., Rettie, A. E., Fowler, D. M., & Miners, J. O. (2017). Pharmacogenomics of CYP2C9: Functional and clinical considerations. *Journal of Personalized Medicine, 8*(1), 1.

Delport, A., & Hewer, R. (2022). The amyloid precursor protein: A converging point in Alzheimer's disease. *Molecular Neurobiology, 59*(7), 4501–4516.

Dhianawaty, D., Atik, N., Dwiwina, R. G., & Muda, I. (2022). Preliminary identification and quantification of four secondary metabolites, total tannin and total flavonoid contents in guava fruit ethanol extract. *Pharmacognosy Journal*, 14*(2),* 1-8.

Djedjibegovic, J., Marjanovic, A., Panieri, E., & Saso, L. (2020). Ellagic acid-derived urolithins as modulators of oxidative stress. *Oxidative Medicine and Cellular Longevity, 2020,* 1234567.

El-Wetidy, M. S., Ahmad, R., Rady, I., Helal, H., Rady, M. I., Vaali-Mohammed, M. A., Al-Khayal, K., Traiki, T. B., & Abdulla, M. H. (2021). Urolithin A induces cell cycle arrest and apoptosis by inhibiting Bcl-2, increasing p53-p21 proteins and reactive oxygen species production in colorectal cancer cells. *Cell Stress and Chaperones, 26,* 473–493.

Faitg, J., D'Amico, D., Rinsch, C., & Singh, A. (2024). Mitophagy activation by urolithin A to target muscle aging. *Calcified Tissue International,* 114(1), 53-59.

Faki, Y., & Er, A. (2021). Different chemical structures and physiological/pathological roles of cyclooxygenases. *Rambam Maimonides Medical Journal, 12*(1), e000x.

Favari, C., De Alvarenga, J. F. R., Sánchez-Martínez, L., Tosi, N., Mignogna, C., Cremonini, E., Manach, C., Bresciani, L., Del Rio, D., & Mena, P. (2024). Factors driving the inter-individual variability in the metabolism and bioavailability of (poly)phenolic metabolites: A systematic review of human studies. *Redox Biology, 39,* 103095.

Feng, R., Zhou, X., Or, P. M., Ma, J. Y., Tan, X. S., Fu, J., Ma, C., Shi, J. G., Che, C. T., & Wang, Y. (2012). Enzyme kinetic and molecular docking studies on the metabolic interactions of 1-hydroxy-2,3,5-trimethoxy-xanthone, isolated from *Halenia elliptica* D.

Don, with model probe substrates of human cytochrome P450 enzymes. *Phytomedicine, 19*(12), 1125–1133.

Franceschi, C., Garagnani, P., Morsiani, C., Conte, M., Santoro, A., Grignolio, A., Monti, D., Capri, M., & Salvioli, S. (2018). The continuum of aging and age-related diseases: Common mechanisms but different rates. *Frontiers in Medicine, 5*, 61.

Frishman, A., & Ronceray, P. (2020). Learning force fields from stochastic trajectories. *Physical Review X, 10*(2), 021009.

Gaillard, T. (2018). Evaluation of AutoDock and AutoDock Vina on the CASF-2013 benchmark. *Journal of Chemical Information and Modeling, 58*(8), 1697–1706.

Gandhi, S. E., Zerenner, T., Nodehi, A., Lawton, M. A., Marshall, V., Al-Hajraf, F., Grosset, K. A., Morris, H. R., Hu, M. T., & Ben-Shlomo, Y. (2024). Motor complications in Parkinson's disease: Results from 3,343 patients followed for up to 12 years. *Movement Disorders Clinical Practice, 11*(6), 686–697.

Gangwal, R. P., Das, N. R., Thanki, K., Damre, M. V., Dhoke, G. V., Sharma, S. S., Jain, S., & Sangamwar, A. T. (2014). Identification of p38α MAP kinase inhibitors by pharmacophore-based virtual screening. *Journal of Molecular Graphics and Modelling, 49*, 18–24.

García-Villalba, R., Giménez-Bastida, J. A., Cortés-Martín, A., Ávila-Gálvez, M. Á., Tomás-Barberán, F. A., Selma, M. V., Espín, J. C., & González-Sarrías, A. (2022a). Urolithins: A comprehensive update on their metabolism, bioactivity, and associated gut microbiota. *Molecular Nutrition & Food Research, 66*(21), 2101019.

García-Villalba, R., Giménez-Bastida, J. A., Cortés-Martín, A., Ávila-Gálvez, M. Á., Tomás-Barberán, F. A., Selma, M. V., Espín, J. C., & González-Sarrías, A. (2022b). Urolithins: A comprehensive update on their metabolism, bioactivity and associated gut microbiota. *Molecular Nutrition & Food Research, 66*(21), 2101019.

García-Villalba, R., Selma, M. V., Espín, J. C., & Tomás-Barberán, F. A. (2019). Identification of novel urolithin metabolites in human feces and urine after the intake of a pomegranate extract. *Journal of Agricultural and Food Chemistry, 67*(40), 11099–11107.

Gartner III, T. E., & Jayaraman, A. (2019). Modeling and simulations of polymers: A roadmap. *Macromolecules, 52*(3), 755–786.

Gasteiger, J., & Marsili, M. (1980). Iterative partial equalization of orbital electronegativity: A rapid access to atomic charges. *Tetrahedron, 36*(22), 3219–3228.

Gasteiger, J., Yeshwanth, C., & Günnemann, S. (2021). Directional message passing on molecular graphs via synthetic coordinates. *Advances in Neural Information Processing Systems, 34*, 15421–15433.

George, N., AbuKhader, M., Al Balushi, K., Al Sabahi, B., & Khan, S. A. (2023). An insight into the neuroprotective effects and molecular targets of pomegranate (*Punica granatum*) against Alzheimer's disease. *Nutritional Neuroscience, 26*(10), 975–996.

Goodsell, D. S., Zardecki, C., Di Costanzo, L., Duarte, J. M., Hudson, B. P., Persikova, I., Segura, J., Shao, C., Voigt, M., & Westbrook, J. D. (2020). RCSB Protein Data Bank: Enabling biomedical research and drug discovery. *Protein Science, 29*(1), 52–65.

Gu, D., Andreev, K., & Dupre, M. E. (2021). Major trends in population growth around the world. *China CDC Weekly, 3*(28), 604–610.

Hadia, R., Singh, V., Solanki, N., Sharma, S., Saggu, V., Sajan, C., Trivedi, R., Kardani, S., Baile, S., & Rajput, H. S. (2024). Unlocking the clinical significance of cytochrome P450 enzymes. *International Journal of Pharmaceutical Investigation, 14*(1), 1–10.

Halgren, T. A. (1996). Merck molecular force field. I. Basis, form, scope, parameterization, and performance of MMFF94. *Journal of Computational Chemistry, 17*(5–6), 490–519.

Haller, V., Nahidino, P., Forster, M., & Laufer, S. A. (2020). An updated patent review of p38 MAP kinase inhibitors (2014–2019). *Expert Opinion on Therapeutic Patents, 30*(6), 453–466.

Hampel, H., Hardy, J., Blennow, K., Chen, C., Perry, G., Kim, S. H., Villemagne, V. L., Aisen, P., Vendruscolo, M., & Iwatsubo, T. (2021). The amyloid-β pathway in Alzheimer's disease. *Molecular Psychiatry, 26*(10), 5481–5503.

Harinie, S. (2022). An in-silico study of phytochemicals of *Andrographis paniculata* and their derivatives as inhibitors of NS3 helicase, NS3 protease and NS5 methyl transferase of Dengue virus. *Global Journal of Innovation in Medical Sciences, 1*(1), 45–57.

Hasheminezhad, S. H., Boozari, M., Iranshahi, M., Yazarlu, O., Sahebkar, A., Hasanpour, M., & Iranshahy, M. (2022). A mechanistic insight into the biological activities of urolithins as gut microbial metabolites of ellagitannins. *Phytotherapy Research, 36*(1), 112–146.

Hassanein, E. H., Sayed, A. M., Hussein, O. E., & Mahmoud, A. M. (2020). Coumarins as modulators of the Keap1/Nrf2/ARE signaling pathway. *Oxidative Medicine and Cellular Longevity, 2020*, Article ID 2345678.

Hayani, S., Thiruvalluvar, A. A., Baba, Y. F., Rodi, Y. K., Muthunatesan, S., Chahdi, F. O., Mague, J. T., El Ibrahimi, B., Sebbar, N. K., & Essassi, E. M. (2021). Synthesis, structure elucidation, Hirshfeld surface analysis, DFT, molecular docking and Monte Carlo simulation of new quinoline-4-carboxylate derivatives. *Journal of Molecular Structure, 1234*, 130195.

Hollingsworth, S. A., & Dror, R. O. (2018). Molecular dynamics simulation for all. *Neuron, 99*(6), 1129–1143.

Huang, J., Zhang, M., Chen, Y., Sun, Y., Gao, Z., Li, Z., Zhang, G., Qin, Y., Dai, X., & Yu, X. (2023). Urolithin A ameliorates obesity-induced metabolic cardiomyopathy in mice via mitophagy activation. *Acta Pharmacologica Sinica*, *44*(2), 321–331.

Huang, X., Hussain, B., & Chang, J. (2021). Peripheral inflammation and blood–brain barrier disruption: Effects and mechanisms. *CNS Neuroscience & Therapeutics, 27*(1), 36–47.

Hui, Y., Smith, B., Mortensen, M. S., Krych, L., Sørensen, S. J., Greisen, G., Krogfelt, K. A., & Nielsen, D. S. (2021). The effect of early probiotic exposure on the preterm infant gut microbiome development. *Gut Microbes, 13*(1), Article 1951113.

Hurley, D. J., Nixon, M. S., & Carter, J. N. (2005). Force field feature extraction for ear biometrics. *Computer Vision and Image Understanding, 98*(3), 491–512.

Iglesias-Aguirre, C. E., García-Villalba, R., Beltrán, D., Frutos-Lisón, M. D., Espín, J. C., Tomás-Barberán, F. A., & Selma, M. V. (2023). Gut bacteria involved in ellagic acid

metabolism to yield human urolithin metabotypes revealed. *Journal of Agricultural and Food Chemistry, 71*(9), 4029–4035.

Irrgang, M. E., Davis, C., & Kasson, P. M. (2022). gmxapi: A GROMACS-native Python interface for molecular dynamics with ensemble and plugin support. *PLOS Computational Biology, 18*(2), e1009835.

Ito, H. (2011). Metabolites of the ellagitannin geraniin and their antioxidant activities. *Planta Medica, 77*(11), 1110–1115.

Ito, H., Iguchi, A., & Hatano, T. (2008). Identification of urinary and intestinal bacterial metabolites of ellagitannin geraniin in rats. *Journal of Agricultural and Food Chemistry, 56*(2), 393–400.

Jain, P., Satija, J., & Sudandiradoss, C. (2023). Discovery of andrographolide hit analog as a potent cyclooxygenase-2 inhibitor through consensus MD-simulation, electrostatic potential energy simulation and ligand efficiency metrics. *Scientific Reports, 13*(1), 8147.

Jiao, J., Yang, Y., Wu, Z., Li, B., Zheng, Q., Wei, S., Wang, Y., & Yang, M. (2019). Screening cyclooxygenase-2 inhibitors from *Andrographis paniculata* to treat inflammation based on bio-affinity ultrafiltration coupled with UPLC-Q-TOF-MS. *Fitoterapia, 137*, 104259.

Ju, Z., Li, M., Xu, J., Howell, D. C., Li, Z., & Chen, F. E. (2022). Recent development on COX-2 inhibitors as promising anti-inflammatory agents: The past 10 years. *Acta Pharmaceutica Sinica B, 12*(6), 2790–2807.

Kallio, T., Kallio, J., Jaakkola, M., Mäki, M., Kilpeläinen, M., & Virtanen, V. (2013). Urolithins display both antioxidant and pro-oxidant activities depending on assay system and conditions. *Journal of Agricultural and Food Chemistry, 61*(45), 10720–10729.

Ki, M. R., Youn, S., Kim, D. H., & Pack, S. P. (2024). Natural compounds for preventing age-related diseases and cancers. *International Journal of Molecular Sciences, 25*(14), 7530.

Kim, I. J., & Na, H. (2022). An efficient algorithm calculating common solvent accessible volume. *Plos One, 17*(3), e0265614.

Kim, S., Thiessen, P. A., Bolton, E. E., Chen, J., Fu, G., Gindulyte, A., Han, L., He, J., He, S., & Shoemaker, B. A. (2016). PubChem substance and compound databases. *Nucleic Acids Research, 44*(D1), D1202–D1213.

Krivanek, T. J., Gale, S. A., McFeeley, B. M., Nicastri, C. M., & Daffner, K. R. (2021). Promoting successful cognitive aging: A ten-year update. *Journal of Alzheimer's Disease, 81*(3), 871–920.

Kujawska, M., Jourdes, M., Kurpik, M., Szulc, M., Szaefer, H., Chmielarz, P., Kreiner, G., Krajka-Kuźniak, V., Mikołajczak, P. Ł., & Teissedre, P. L. (2019). Neuroprotective effects of pomegranate juice against Parkinson's disease and presence of ellagitannins-derived metabolite—Urolithin A—in the brain. *International Journal of Molecular Sciences, 21*(1), Article 202.

Kuppusamy, U. R., & Arumugam, B. (2023). Novel plant bioactives, their antiaging potencies: Reality and promises. In *Plant Bioactives as Natural Panacea Against Age-Induced Diseases* (pp. 359–386). Elsevier.

Okigbo, R., & Anyaegbu, C. (2021). Underutilized plants of Africa. *Journal of Biology and Nature, 13*(2), 1–17.

Okoro, N. O., Odiba, A. S., Osadebe, P. O., Omeje, E. O., Liao, G., Fang, W., Jin, C., & Wang, B. (2021). Bioactive phytochemicals with anti-aging and lifespan extending potentials in *Caenorhabditis elegans*. *Molecules, 26*(23), 7323.

Okumura, T. (2021). The potential as new treatment agent of Urolithin-A metabolized from ellagic acid by gut microbiota in cancer. *Juntendo Medical Journal, 67*(2), 131–139.

Olaoye, F. S., Ezeoguine, J., & Uku, F. (2020). Exploring the potentials of underutilized African nuts (black walnuts and almonds) for nutrition and diseases. *American Journal of Food Sciences and Nutrition, 2*(1), 21–31.

Onishi, M., Yamano, K., Sato, M., Matsuda, N., & Okamoto, K. (2021). Molecular mechanisms and physiological functions of mitophagy. *The EMBO Journal, 40*(3), e104705.

Park, S. H., Lee, D. H., Lee, D. H., & Jung, C. H. (2024). Scientific evidence of foods that improve the lifespan and healthspan of different organisms. *Nutrition Research Reviews, 37*(1), 169–178.

Pasieka, A., Panek, D., Szałaj, N., Espargaró, A., Więckowska, A., Malawska, B., Sabaté, R., & Bajda, M. (2021). Dual inhibitors of amyloid-β and tau aggregation with amyloid-β disaggregating properties: Extended *in cellulo, in silico*, and kinetic studies of multifunctional anti-Alzheimer's agents. *ACS Chemical Neuroscience, 12*(11), 2057–2068.

Prabhu, S., Molath, A., Choksi, H., Kumar, S., & Mehra, R. (2021). Classifications of polyphenols and their potential application in human health and diseases. *International Journal of Physiology, Nutrition and Physical Education, 6*(1), 293–301.

Pradhan, M. R. (2017*). Biomolecular Hydration in Protein-Protein Interaction, Protein Stability and Aggregation and Lead Optimization: Computational Studies (Doctoral Dissertation).* https://scholar.google.com

Quinn, P. M., Moreira, P. I., Ambrósio, A. F., & Alves, C. H. (2020). PINK1/PARKIN signalling in neurodegeneration and neuroinflammation. *Acta Neuropathologica Communications, 8*(1), 189.

Raina, J., Firdous, A., Singh, G., Kumar, R., & Kaur, C. (2024). Role of polyphenols in the management of diabetic complications. *Phytomedicine*, 122, 155155.

Rehman, S., Aatif, M., Rafi, Z., Khan, M. Y., Shahab, U., Ahmad, S., & Farhan, M. (2022). Effect of non-enzymatic glycosylation in the epigenetics of cancer. *Antioxidants & Redox Signaling*, *83*, 543–555.

Roda, A. R., Serra-Mir, G., Montoliu-Gaya, L., Tiessler, L., & Villegas, S. (2022). Amyloid-beta peptide and tau protein crosstalk in Alzheimer's disease. *Neural Regeneration Research, 17*(8), 1666–1674.

Roduner, E., & Krüger, T. P. (2022). The origin of irreversibility and thermalization in thermodynamic processes. *Physics Reports, 944*, 1–43.

Rogers, A., Grieve, K., MacDonald, T. M., & Nishioka, S. (2020). COX-2 *Inhibitors: Communication of Accumulating Risk Evidence and a Product Withdrawal. In*

Communicating About Risks and Safe Use of Medicines: Real Life And Applied Research (pp. 131-146). Singapore: Springer Singapore. https://scholar.google.com

Romo-Vaquero, M., García-Villalba, R., González-Sarrías, A., Beltrán, D., Tomás-Barberán, F. A., Espín, J. C., & Selma, M. V. (2015). Interindividual variability in the human metabolism of ellagic acid: Contribution of *Gordonibacter* to urolithin production. *Journal of Functional Foods, 17*, 785–791.

Rubavathy, S. E., & Prakash, M. (2025). Computational insights in repurposing a cardiovascular drug for Alzheimer's disease: The role of aromatic amino acids in stabilizing the drug through π–π stacking interaction. *Physical Chemistry Chemical Physics, 27*(2), 1071–1082.

Rungratanawanich, W., Qu, Y., Wang, X., Essa, M. M., & Song, B. J. (2021). Advanced glycation end products and other adducts in aging-related diseases and alcohol-mediated tissue injury. *Experimental & Molecular Medicine, 53*(2), 168–188.

Sailah, I., Tumilaar, S. G., Lombogia, L. T., Celik, I., & Tallei, T. E. (2021). Molecular docking and dynamics simulations study of selected phytoconstituents of *Pangi* (*Pangium edule* Reinw) leaf as anti-SARS-CoV-2. *Philippine Journal of Science, 150*(5), 2021.

Scalbert, A., Morand, C., Manach, C., & Rémésy, C. (2002). Absorption and metabolism of polyphenols in the gut and impact on health. *Biomedicine & Pharmacotherapy, 56*(6), 276–282.

Schepens Niemiec, S. L., Lee, E., Saunders, R., Wagas, R., & Wu, S. (2023). Technology for activity participation in older people with mild cognitive impairment or dementia: Expert perspectives and a scoping review. *Disability and Rehabilitation: Assistive Technology, 18*(8), 1555–1576.

Shi, M., & McHugh, K. J. (2023). Strategies for overcoming protein and peptide instability in biodegradable drug delivery systems. *Advanced Drug Delivery Reviews*, 114904.

Shi, T., & Dansen, T. B. (2020). Reactive oxygen species induced p53 activation: The DNA damage, redox signaling, or both? *Antioxidants & Redox Signaling, 33*(12), 839–859.

Siddarth, P., Li, Z., Miller, K. J., Ercoli, L. M., Merril, D. A., Henning, S. M., Heber, D., & Small, G. W. (2020). Randomized placebo-controlled study of the memory effects of

pomegranate juice in middle-aged and older adults. *The American Journal of Clinical Nutrition, 111*(1), 170–177.

Silman, I. (2021). The multiple biological roles of the cholinesterases. *Progress in Biophysics and Molecular Biology, 162*, 41–56.

Singh, A., D'Amico, D., Andreux, P. A., Dunngalvin, G., Kern, T., Blanco-Bose, W., Auwerx, J., Aebischer, P., & Rinsch, C. (2022). Direct supplementation with Urolithin A overcomes limitations of dietary exposure and gut microbiome variability in healthy adults to achieve consistent levels across the population. *European Journal of Clinical Nutrition, 76*(2), 297–308.

Singh, A., D'Amico, D., Andreux, P. A., Fouassier, A. M., Blanco-Bose, W., Evans, M., Aebischer, P., Auwerx, J., & Rinsch, C. (2022). Urolithin A improves muscle strength, exercise performance, and biomarkers of mitochondrial health in a randomized trial in middle-aged adults. *Cell Reports Medicine, 3*(5).

Singh, R. D., Avadhesh, A., Sharma, G., Dholariya, S., Shah, R. B., Goyal, B., & Gupta, S. C. (2023). Potential of cytochrome P450, a family of xenobiotic metabolizing enzymes, in cancer therapy. *Antioxidants & Redox Signaling, 38*(10–12), 853–876.

Suez, J., & Elinav, E. (2017). The path towards microbiome-based metabolite treatment. *Nature Microbiology, 2*(6), 1–5.

Tahir, A., Mobeen, B., Hussain, F., Sadiq, A., & Rashid, U. (2024). Pregnenolone derivatives for the treatment of Alzheimer's disease: Synthesis, and in vitro inhibition of amyloid β 1–42 peptide aggregation, acetylcholinesterase and carbonic anhydrase-II. *RSC Advances*, 14(21), 14742-14757.

Verbeke, K. A., Boobis, A. R., Chiodini, A., Edwards, C. A., Franck, A., Kleerebezem, M., Nauta, A., Raes, J., Van Tol, E. A., & Tuohy, K. M. (2015). Towards microbial fermentation metabolites as markers for health benefits of prebiotics. *Nutrition Research Reviews, 28*(1), 42–66.

Walczak-Nowicka, Ł. J., & Herbet, M. (2021). Acetylcholinesterase inhibitors in the treatment of neurodegenerative diseases and the role of acetylcholinesterase in their pathogenesis. *International Journal of Molecular Sciences, 22*(17), 9290.

Weinhäupl, K., Lindau, C., Hessel, A., Wang, Y., Schütze, C., Jores, T., Melchionda, L., Schönfisch, B., Kalbacher, H., & Bersch, B. (2018). Structural basis of membrane protein chaperoning through the mitochondrial intermembrane space. *Cell*, *175*(5), 1365–1379.

World Health Organization. (2017). *World health statistics 2017: Monitoring Health for the SDGs*. Sustainable Development Goals, 7. https://scholar.google.com/

Yang, R., Zha, X., Gao, X., Wang, K., Cheng, B., & Yan, B. (2022). Multi-stage virtual screening of natural products against p38α mitogen-activated protein kinase: Predictive modeling by machine learning, docking study and molecular dynamics simulation. *Heliyon*, *8*(9), 1-10.

Yang, Y., Li, S., Wang, Y., Zhao, Y., & Li, Q. (2022). Protein tyrosine kinase inhibitor resistance in malignant tumors: Molecular mechanisms and future perspective. *Signal Transduction and Targeted Therapy*, *7*(1), 329.

Yuan, L., Zhang, C., Sun, H., Liu, Q., Huang, J., Sheng, L., Lin, B., Wang, J., & Chen, L. (2016). The semi-synthesis of novel andrographolide analogues and anti-influenza virus activity evaluation of their derivatives. *Bioorganic & Medicinal Chemistry Letters*, *26*(3), 769–773.

Yue, J., & López, J. M. (2020). Understanding MAPK signaling pathways in apoptosis. *International Journal of Molecular Sciences*, *21*(7), 2346.

Yun, S., & Guy, H. R. (2011). Stability tests on known and misfolded structures with discrete and all atom molecular dynamics simulations. *Journal of Molecular Graphics and Modelling*, *29*(5), 663–675.

Zagnoli-Vieira, G., & Caldecott, K. W. (2020). Untangling trapped topoisomerases with tyrosyl-DNA phosphodiesterases. *DNA Repair*, *94*, 102900.

Zahrani, N. A. A., El-Shishtawy, R. M., & Asiri, A. M. (2020). Recent developments of gallic acid derivatives and their hybrids in medicinal chemistry: A review. *European Journal of Medicinal Chemistry*, *204*, 112609.

Zarougui, S., Er-rajy, M., Faris, A., Imtara, H., Alshawwa, S. Z., Nasr, F. A., Aloui, M., & Elhallaoui, M. (2023). QSAR, DFT studies, docking molecular and simulation dynamic

molecular of 2-styrylquinoline derivatives through their anticancer activity. *Journal of Saudi Chemical Society, 27*(6), 101728.

Zhang, M., Gui, M., Wang, Z.-F., Gorgulla, C., Yu, J. J., Wu, H., Sun, Z. J., Klenk, C., Merklinger, L., & Morstein, L. (2021). Cryo-EM structure of an activated GPCR–G protein complex in lipid nanodiscs. *Nature Structural & Molecular Biology, 28*(3), 258–267.

Zhang, Y., Chen, H., Li, R., Sterling, K., & Song, W. (2023). Amyloid β-based therapy for Alzheimer's disease: Challenges, successes and future. *Signal Transduction and Targeted Therapy, 8*(1), 248.

Zhang, M., Cui, S., Mao, B., Zhang, Q., Zhao, J., Zhang, H., Tang, X., & Chen, W. (2023). Ellagic acid and intestinal microflora metabolite urolithin A: A review on its sources, metabolic distribution, health benefits, and biotransformation. *Critical Reviews in Food Science and Nutrition, 63*(24), 6900–6922.

Zhao, H., Song, G., Zhu, H., Qian, H., Pan, X., Song, X., Xie, Y., & Liu, C. (2023). Pharmacological effects of urolithin A and its role in muscle health and performance: Current knowledge and prospects. *Nutrients, 15*(20), 4441.

Zhao, M., Ma, J., Li, M., Zhang, Y., Jiang, B., Zhao, X., Huai, C., Shen, L., Zhang, N., & He, L. (2021). Cytochrome P450 enzymes and drug metabolism in humans. *International Journal of Molecular Sciences, 22*(23), 12808.

RESEARCH OUTPUTS

(i) Publications

Massaga, C. A., Raymond, J., Luchemba, L. P., Vianney, S. J. M., & Chacha, M. **(**2024). Computational investigation of Urolithin A binding affinities and dynamics on targets implicated in anti-inflammatory, antioxidant, and neurodegenerative pathways. *Free Radical Biology and Medicine,* 227*, 508–520.*

(ii) Poster presentation